Cell Reports

Article

Hypoxic, glycolytic metabolism is a vulnerability of B-acute lymphoblastic leukemia-initiating cells

Graphical abstract

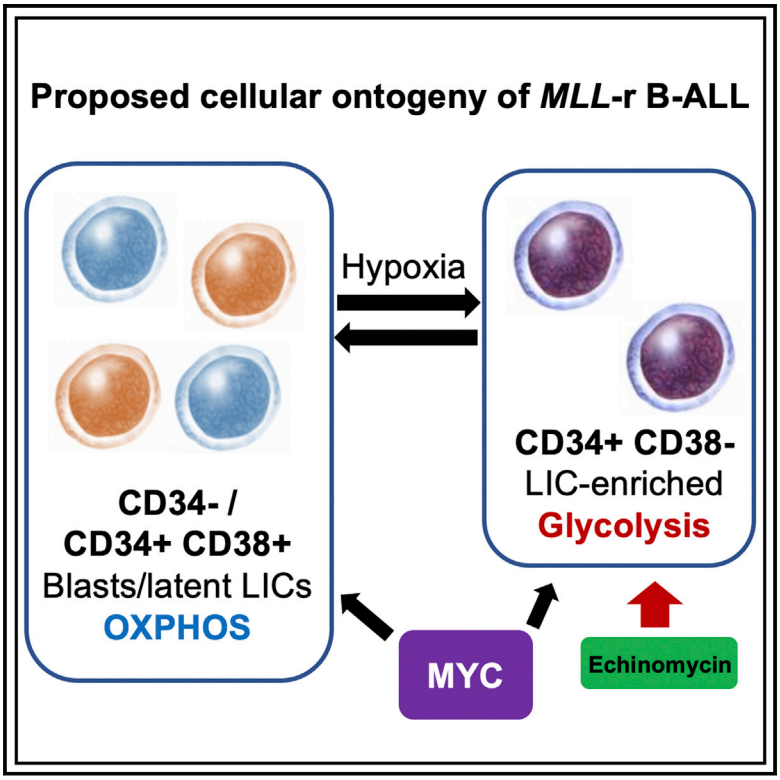

Highlights

- *MLL*-r B-ALL cells are varied, with a defined population enriched in initiating cells
- *MLL*-r B-ALL-initiating cells are plastic, emerging from more differentiated states
- MYC-driven metabolic heterogeneity may provide a therapeutic opportunity

Authors

Vivian Morris, Dahai Wang, Zhiheng Li, ..., George Q. Daley, Edroaldo Lummertz da Rocha, R. Grant Rowe

Correspondence

grant_rowe@dfci.harvard.edu

In brief

Morris et al. use single-cell transcriptomics to identify a candidate-initiating cell in B-acute lymphoblastic leukemia (B-ALL) with rearrangement of the KMT2A/MLL1 locus (MLL-r), finding that this population is plastic and exists in a hypoxic state that can be pharmacologically targeted.

Morris et al., 2022, Cell Reports *39*, 110752
April 26, 2022
https://doi.org/10.1016/j.celrep.2022.110752

CellPress

Cell Reports

CellPress
OPEN ACCESS

Article

Hypoxic, glycolytic metabolism is a vulnerability of B-acute lymphoblastic leukemia-initiating cells

Vivian Morris,[1,15] Dahai Wang,[2,15] Zhiheng Li,[2] William Marion,[1] Travis Hughes,[3,4,5] Patricia Sousa,[1] Taku Harada,[6] Shannan Ho Sui,[7] Sergey Naumenko,[7] Jérémie Kalfon,[4] Prerana Sensharma,[1,2] Marcelo Falchetti,[8] Renan Vinicius da Silva,[8] Tito Candelli,[9] Pauline Schneider,[9] Thanasis Margaritis,[9] Frank C.P. Holstege,[9] Yana Pikman,[5,6] Marian Harris,[5,10] Ronald W. Stam,[9] Stuart H. Orkin,[5,6,11] Angela N. Koehler,[3,4] Alex K. Shalek,[3,4,12,13] Trista E. North,[1,5] Maxim Pimkin,[4,5,6] George Q. Daley,[1,5] Edroaldo Lummertz da Rocha,[14,15] and R. Grant Rowe[1,2,5,6,15,16,*]

[1]Stem Cell Program, Boston Children's Hospital, Boston, MA 02115, USA
[2]Stem Cell Transplantation Program, Department of Hematology, Boston Children's Hospital, Boston, MA 02115, USA
[3]Koch Institute for Integrative Cancer Research, Massachusetts Institute of Technology, Cambridge, MA 02139, USA
[4]Broad Institute of MIT and Harvard, Cambridge, MA 02142, USA
[5]Harvard Medical School, Boston, MA 02115, USA
[6]Cancer and Blood Disorders Center, Dana-Farber Cancer Institute and Boston Children's Hospital, Boston, MA 02115, USA
[7]Harvard Chan Bioinformatics Core, Harvard T.H. Chan School of Public Health, Boston, MA 02115, USA
[8]Graduate Program of Pharmacology, Center for Biological Sciences, Federal University of Santa Catarina, Florianópolis, Santa Catarina 88040-900, Brazil
[9]Princess Máxima Center for Pediatric Oncology, Utrecht, the Netherlands
[10]Department of Pathology, Boston Children's Hospital, Boston, MA 02115, USA
[11]Howard Hughes Medical Institute, Boston, MA 02115, USA
[12]Institute for Medical Engineering & Science, Department of Chemistry, Massachusetts Institute of Technology, Cambridge, MA 02142, USA
[13]Ragon Institute of MGH, MIT, and Harvard, Cambridge, MA 02139, USA
[14]Department of Microbiology, Immunology and Parasitology, Federal University of Santa Catarina, Florianópolis Santa Catarina 88040-900, Brazil
[15]These authors contributed equally
[16]Lead contact
*Correspondence: grant_rowe@dfci.harvard.edu
https://doi.org/10.1016/j.celrep.2022.110752

SUMMARY

High-risk forms of B-acute lymphoblastic leukemia (B-ALL) remain a therapeutic challenge. Leukemia-initiating cells (LICs) self-renew and spark relapse and therefore have been the subject of intensive investigation; however, the properties of LICs in high-risk B-ALL are not well understood. Here, we use single-cell transcriptomics and quantitative xenotransplantation to understand LICs in *MLL*-rearranged (*MLL*-r) B-ALL. Compared with reported LIC frequencies in acute myeloid leukemia (AML), engraftable LICs in *MLL-r* B-ALL are abundant. Although we find that multipotent, self-renewing LICs are enriched among phenotypically undifferentiated B-ALL cells, LICs with the capacity to replenish the leukemic cellular diversity can emerge from more mature fractions. While inhibiting oxidative phosphorylation blunts blast proliferation, this intervention promotes LIC emergence. Conversely, inhibiting hypoxia and glycolysis impairs *MLL*-r B-ALL LICs, providing a therapeutic benefit in xenotransplantation systems. These findings provide insight into the aggressive nature of *MLL*-r B-ALL and provide a rationale for therapeutic targeting of hypoxia and glycolysis.

INTRODUCTION

B-acute lymphoblastic leukemia (B-ALL) is heterogeneous, with certain unfavorable genetic subtypes continuing to bear poor prognosis despite the remarkable progress made in improving overall outcomes. B-ALL with rearrangement of the *KMT2A/MLL1* locus (*MLL*-r) constitutes about 80% of B-ALL of infancy, with incidence diminishing in childhood but later increasing in adulthood (Boissel and Baruchel, 2018). *MLL*-r B-ALL is a very high-risk form of B-ALL, often presenting with high leukemic burden, corticosteroid resistance, and central nervous system infiltration (Pieters et al., 2007). This aggressive clinical behavior is associated with distinctive underlying biology, including coexpression of myeloid markers and a capacity to undergo a B-lymphoid-to-myeloid lineage switch in response to therapy (Pieters et al., 2007). Based on these clinical observations, we hypothesized that the aggressive nature of human *MLL*-r B-ALL is underpinned by a high content of leukemia-initiating cells (LICs) retaining hematopoietic stem cell (HSC)- and multipotent progenitor (MPP)-like differentiation states and multipotency programs.

LICs possess the capability to fully reconstitute fulminant leukemia at relapse or, experimentally, upon xenotransplantation. This definition was initially formed based on the foundational observation that only a small, specific minority of human acute

myeloid leukemia (AML) cells could sustainably engraft immunodeficient mice, establishing engraftment in xenotransplantation as the gold standard to detect LICs (Lapidot et al., 1994). Although LICs have been previously accepted to be phenotypically primitive and rare, recent advances suggest that such early paradigms of LIC biology might be subject to revision. The use of improved immunodeficient mouse strains with heightened sensitivity for human stem cell engraftment has revealed that LICs are heterogeneous in their oncogenetics and can be detected in multiple differentiation states in both AML and ALL, although the common factors that maintain diverse LIC states are not well understood (Anderson et al., 2011; Aoki et al., 2015; McKenzie et al., 2019; Sarry et al., 2011). These findings could explain the limited clinical success of interventions targeting LICs despite intensive investigation of their molecular vulnerabilities (Pollyea and Jordan, 2017). Much of this investigation has focused on metabolic vulnerabilities, particularly oxidative phosphorylation as an LIC dependency in AML (Lagadinou et al., 2013).

Although findings illustrating LIC heterogeneity have led to reassessment of classical models of leukemic ontogeny, it remains generally accepted that leukemia cells are functionally heterogeneous with variable xenotransplantation capacities. Since the frequency of engraftable cells within individual leukemias—a readout of LIC content—is reproducibly of prognostic importance, better understanding of determinants of the LIC state has therapeutic potential (Monaco et al., 2004; Paczulla et al., 2017). Here, we use single-cell RNA sequencing (scRNA-seq) combined with xenotransplantation to define LICs in *MLL*-r B-ALL. We demonstrate that, although LICs are enriched in the most phenotypically primitive fraction of *MLL*-r B-ALL, they can emerge from blast populations with more differentiated immunophenotypes to reconstitute the full leukemic cellular diversity. Although most blasts utilize oxidative phosphorylation for expansion, primitive *MLL*-r B-ALL LICs can emerge from more differentiated populations by acquisition and maintenance of a relatively quiescent, hypoxic, glycolytic phenotype that can be therapeutically targeted. Consistent with its global effects on cancer cell metabolism, MYC plays a dual role in regulating both metabolic pathways in multiple strata of leukemic ontogeny (Fang et al., 2019; Lee et al., 2017). Together, our findings define mechanisms of LIC integrity and advance a candidate approach to therapy for high-risk forms of B-ALL.

RESULTS

Single-cell RNA sequencing identifies candidate LICs in *MLL*-r B-ALL

The ability to switch lineage from B-lymphoid to myeloid at relapse suggests that *MLL*-r B-ALL LICs possess multipotency (Pieters et al., 2007; Rossi et al., 2012). To determine whether we can capture this property of normal HSCs and MPPs in *MLL*-r B-ALL, we aimed to elicit both B-lymphoid and myeloid differentiation at the single-cell level. To this end, we employed early-passage patient-derived xenografts (PDXs) and primary patient cells. Upon xenotransplantation, human B-ALL cells infiltrated the liver, spleen, lymph nodes, and central nervous system of unconditioned non-obese diabetic (NOD).Cg-*Prkdc*^{scid}*Il2rg*^{tm1Wjl} (NSG) mice, recapitulating the clinical behavior of *MLL*-r B-ALL in humans (Figure S1A). *MLL*-r B-ALL cells nearly uniformly expressed the B-cell marker CD19, with rare cells expressing the myeloid marker CD33 while maintaining the morphology of immature lymphoblasts (Figure S1B). Following culture in a pro-myeloid and lymphoid MS5 stromal system, single *MLL*-r B-ALL cells showed B-lymphoid and myeloid multipotent differentiation outcomes with detection of *MLL* fusions in all populations (Figures S1C–S1E; Issaad et al., 1993; Doulatov et al., 2010). In this system, *MLL*-r B-ALL cells were highly clonogenic (Figure S1F). These findings were consistent with a previously reported dependence on stromal co-culture for B-ALL expansion (Pal et al., 2016). These results demonstrate single-cell-level B-lymphoid and myeloid potential consistent with multipotent HSC- and MPP-like programs in *MLL*-r B-ALL.

With the aim of identifying candidate LICs, we performed scRNA-seq using two human *MLL*-r B-ALL specimens (*MLL-AF4* and *MLL-ENL*) with tracking of multipotency signatures. We obtained 11,709 viable, human CD45$^+$ single cells for analysis after performing quality controls. Unsupervised graph-based clustering of the combined datasets identified 12 transcriptional groups with unique signatures, with partial overlap of the two specimens (Figures 1A and 1B). Using the SingleCellNet algorithm to compare each cluster with normal adult bone marrow hematopoietic benchmarks, we found that most cells classified strongly as pro-B cells (Figure 1C; Tan and Cahan, 2019; van Galen et al., 2019). By tracking reported hematopoietic stem and progenitor cell (HSPC) signatures, transcriptional clusters 5 and 10 were advanced as candidate LIC-enriched populations; however, only cluster 10 had consistent enrichment of both HSPC signatures and contributions from both specimens (Figure 1D; Ivanova et al., 2002; Jaatinen et al., 2006). Compared with other populations, this population showed relatively low pre-B classification, concomitant classical dendritic and promonocyte signatures, and progenitor classification suggestive of relative dedifferentiation and potential multipotency (Figure 1C). Furthermore, to further define differentiation state, we classified these *MLL*-r B-ALL cells against known HSPC benchmarks in another published scRNA-seq dataset, finding that cluster 10 showed relatively weak pre-B/NK classification—indicative of a lesser degree of lineage commitment—with strong multi-lymphoid progenitor (MLP) classification relative to other clusters, consistent with a less differentiated, multipotent-like state, as supported by consistent expression of HSPC signatures (Figures 1D and 1E; Pellin et al., 2019).

With the aim of isolating LIC-enriched clusters, we analyzed the expression of cell surface markers. We found that the HSPC marker CD34 was widely expressed, but the candidate LIC-enriched cluster 10 showed low expression of the committed progenitor marker CD38, further suggestive of a multipotent-like state, along with its relatively low B-cell commitment and consistent HSPC classification (Figure 1F). These cells expressed the B-cell markers CD86, CD79A, and CD24 and the monocyte marker CD58, suggestive of mixed lineage potential (Figure 1F). Given these findings and considering the B-lymphoid and myeloid multipotency programs of *MLL*-r B-ALL, we analyzed expression of CD34 and CD38 as well as the additional primitive human HSPC markers CD90

CellPress
OPEN ACCESS

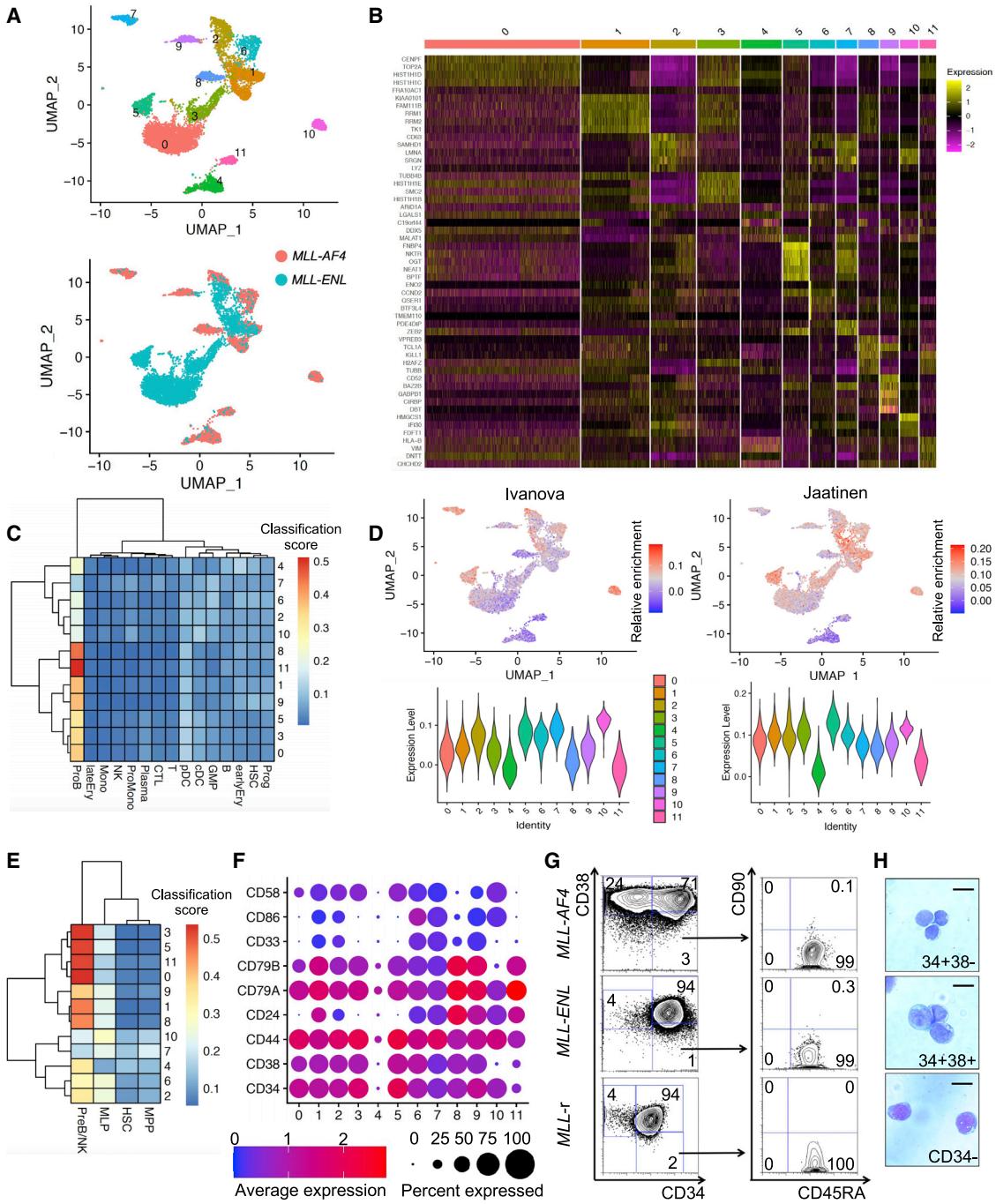

Figure 1. Single-cell heterogeneity of *MLL*-r B-ALL

(A) Human CD45^{+} *MLL*-r B-ALL cells were isolated from peripheral blood and analyzed by scRNA-seq. A combined uniform manifold approximation and projection (UMAP) including both specimens was used to visualize 12 populations with clustering (top) and contribution by specimen (bottom) shown.

(B) Heatmap showing differential transcript expression across each cluster in both combined specimens.

(C) Single cells were classified against a benchmark human bone marrow scRNA-seq dataset (van Galen et al., 2019).

(D) Enrichment of the indicated HSPC signatures was quantified across each cell and visualized using UMAP, with violin plots showing expression of the signature-associated scores.

(E) Single-cell transcriptomes were classified against benchmark HSPC and differentiated populations from a published dataset (Pellin et al., 2019).

(F) The expression of the indicated cell surface markers in each population is shown.

(G) Representative flow cytometry distributions of cells using the indicated markers.

(H) The indicated populations were isolated from representative leukemic marrow (*MLL-AF4*) by fluorescence-activated cell sorting (FACS) and morphology examined following May-Grunwald-Giemsa staining (scale bars represent 10 μm).

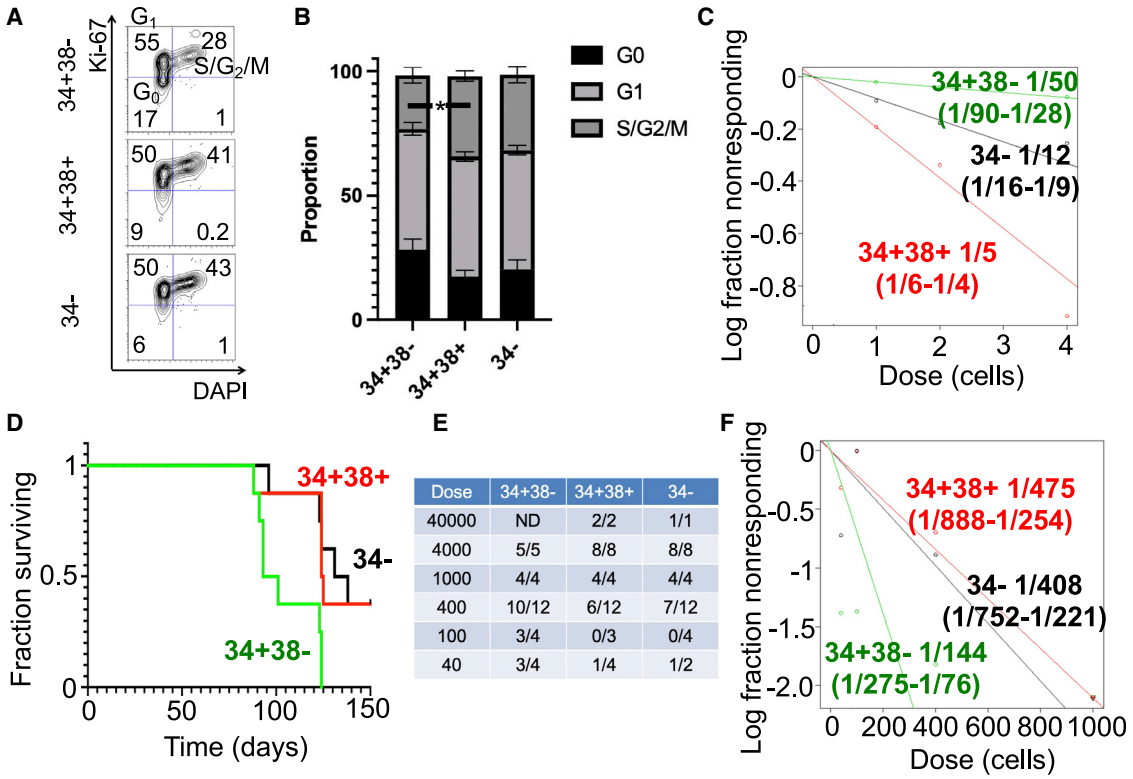

Figure 2. Functional hierarchy in *MLL*-r B-ALL

(A and B) The indicated populations were isolated by FACS and cell cycle analyzed by flow cytometry. Cell cycle distribution of each population was quantified (results aggregated over two independent experiments; n = 11 xenografted mice tested; *p < 0.05 by one-way ANOVA, results show mean ± SEM).

(C) The indicated populations were sorted onto MS5 stromal layers at doses of 1, 2, or 4 cells per well. After 4 weeks, outgrowths at each dose were tabulated and progenitor cell content quantified by limiting dilution analysis. Estimated progenitor cell frequency is presented. Results are aggregated over two independent experiments (for 34+38− versus 34+38+, $X^2 = 64.3$, $p = 1 \times 10^{-15}$; for 34+38− versus 34−, $X^2 = 14.9$, $p = 0.0001$; for 34+38+ versus 34−, $X^2 = 18.1$, $p = 0.00002$).

(D) Four hundred cells of the indicated fractions were xenotransplanted into unconditioned NSG recipients and the incidence of terminal leukemia monitored (results aggregated over two independent transplantation experiments; p = 0.008 for 34+38− versus 34+38+, p = 0.005 for 34+38− versus 34−, and p = 0.9 for 34+38+ versus 34− comparisons by log rank test).

(E) NSG mice were transplanted with the indicated doses of cells from each population and the incidence of terminal leukemia quantified at each dose aggregated over four experiments including two patient donors (see Table S2).

(F) LIC content of each population was quantified by *in vivo* limiting dilution analysis. Results are aggregated over four independent xenotransplantation experiments including two leukemias (for 34+38− versus 34+38+, $X^2 = 7.7$, $p = 0.006$; for 34+38− versus 34−, $X^2 = 6$, $p = 0.01$; for 34+38+ versus 34−, $X^2 = 0.1$, $p = 0.7$).

and CD45RA by flow cytometry. We found that *MLL*-r B-ALLs generally contained three distinguishable populations that we designated based on their surface immunophenotype: rare, undifferentiated $CD34^+$ $CD38^-$ $CD90^-$ $CD45RA^+$ cells (34+38−) with an MLP-like surface profile consistent with the observed scRNA-seq classification; more abundant, progenitor-like $CD34^+$ $CD38^+$ cells (34+38+); and the remaining $CD34^-$ blasts, all of which could be readily sorted from multiple leukemias (34−; Figures 1G, 1H, and S1G). Using additional scRNA-seq datasets, we confirmed evidence of similar hierarchical organization of *MLL*-r B-ALL and possibly *BCR-ABL*-driven B-ALL, although with differing ontogeny in the latter case (Figures S2A–S2I; Candelli et al., 2022; Chen et al., 2021; Witkowski et al., 2020). In line with this finding, using RNA-seq of fluorescence-activated cell sorting (FACS)-purified populations, we found that the 34+38− fraction bore the strongest primitive HSPC signature (Figures S2J and S2K). These findings are suggestive of a phenotypically primitive, LIC-enriched population in *MLL*-r B-ALL.

Functional cellular heterogeneity in *MLL*-r B-ALL

Since LICs are typically quiescent relative to other blasts, we first analyzed cell cycle status (Guan et al., 2003; Saito et al., 2010; Terpstra et al., 1996). First, using PDX cells, we found that the MLP-like, 34+38− fraction contained the highest proportion of cells in G_0 phase (Figures 2A and 2B). Next, we used MS5 assays to quantify leukemic progenitors, finding that more actively cycling 34+38+ cells possessed the highest frequency of short-term clonogenic cells (Figure 2C). We next used limiting dilution xenotransplantation to quantify bona fide LICs (Hu and Smyth, 2009). Using the onset of terminal leukemia as our endpoint, as we initially hypothesized, we first observed that unfractionated human *MLL*-r B-ALL possessed a remarkably high frequency of LICs (1/426 engrafting cells [1/1,417–1/128 95%

confidence interval]) compared with AML (347-fold more frequent than the most efficiently engrafting AML reported previously; Sarry et al., 2011). Upon fractionation, we found that the MLP-like 34+38− population caused leukemia with the shortest latency and contained the highest frequency of engrafting LICs (Figures 2D–2F; Table S2). To exclude an artifactual effect of the PDX system, we corroborated this finding using primary cells sorted from patient peripheral blood (Figures S1H and S1I). These findings indicate that the 34+38− fraction of human *MLL*-r B-ALL is enriched in engraftable LICs.

Latent *MLL*-r B-ALL LICs in 34− and 34+38+ fractions

Although the 34+38− fraction contained abundant LICs, we observed that terminal leukemia also developed in recipients of the 34+38+ and 34− fractions, albeit at lower efficiency (Figures 2D–2F, S1H, and S1I). When we compared the cellular content of leukemia derived from 34+38−, 34+38+, and 34− PDX cells, we found that the full diversity emerged from each source in the terminal disease (Figures 3A and 3B). Moreover, by secondary xenotransplantation, we found that leukemia derived from each source contained serially transplantable LICs (Figure 3C). To directly observe this effect during leukemic reconstitution *in vivo*, we transplanted the least phenotypically primitive 34− cells into NSG mice and isolated bone marrow at defined time points prior to the expected onset of terminal leukemia, finding that 34− cells gradually replenished the $CD34^+$ compartment, suggestive of latent LIC potential (Figures 3D and 3E). Consistent with these xenotransplantation findings, following 4 weeks of culture on MS5 stroma, we found that all input populations could initiate colonies at similar frequencies (Figures S3A and S3B).

To further understand these findings, we cultured sorted populations of 34+38−, 34+38+, and 34− cells on MS5 stroma and monitored population flux. We observed that the content of cultures derived from 34+38+, 34+38−, and 34− cells showed similar $CD34^+$ content by 15 days (Figures S3C and S3D). We observed similar cell state plasticity in primary patient blasts *in vivo* and in culture (Figures S4A–S4D). To control for possible effects of sorting impurities impacting plasticity readouts, we observed cell state plasticity down to the single-cell level using primary patient cells, where we also observed latent myeloid potential in single-cell clones from all phenotypic populations (Figures S4E–S4H).

Finally, to track surface-marker profile and primitive stem cell signatures, we used single-cell cellular indexing of transcriptomes by sequencing (CITE-seq). With this approach, we found that cells with primitive HSPC signatures were present throughout ontogeny, suggesting that cells with the least primitive differentiation states can bear latent stem cell signatures (Figure 3F). Together, these data form a basis for the observed emergence of LICs from more mature populations.

MYC-mediated heterogeneity and plasticity of LICs

We aimed to understand the mechanistic determinants of the *MLL*-r B-ALL LIC state. To this end, we queried the transcriptional profile of phenotypically immature, LIC-enriched 34+38− cells relative to other populations. Moreover, to uncover signatures associated with leukemic engraftment and reconstitution, we also evaluated the profile of mature 34− blasts as they were actively reconstituting the cellular diversity following xenotransplantation ("34−r" cells) versus 34− cells—with the same apparent differentiation state—engrafted at steady state in the presence of other populations (Figure 4A). We found that 34+38−, 34−, and 34−r cells showed markedly divergent transcriptional profiles by RNA-seq, despite the identical immunophenotypes of 34− and 34−r cells (Figure 4B). We noticed that the divergent transcriptional profiles were indicative of variability in metabolic state, with LIC-enriched 34+38− cells showing signatures of hypoxia and glycolysis, and actively reconstituting 34−r cells showing signatures of oxidative phosphorylation and MYC target gene expression (Figure 4C). By performing chromatin immunoprecipitation with sequencing (ChIP-seq) in the B-lymphoid and myeloid *MLL*-r cell line MV4;11 and the *MLL*-r B-ALL cell line RS4;11, we found that transcripts encoded by genes bound by MYC were enriched in 34−r cells, suggestive of a MYC-driven engraftment and reconstitution process (Figure 4D; Lange et al., 1987). Moreover, in a publicly available dataset, we observed that MLL-AF4 bound the *MYC* locus in human HSPCs (Figure S5A).

Since MYC is a central regulator of cancer cell metabolism, we treated cells with IBET-151, a BET bromodomain inhibitor that decreases MYC activity known to impair leukemic growth and monitored B-ALL reconstitution (Dawson et al., 2011; Fang et al., 2019; Lee et al., 2017). As expected, we found that IBET-151 diminished MYC levels (Figure 4E). Treatment of 34− cells either in culture or *in vivo* with IBET-151 blocked the acquisition of the $CD34^+$ state, consistent with a role for MYC in mediating the reconstitution process (Figures 4F–4I). We next generated a doxycycline-inducible, GFP-tagged lentiviral vector for ectopic MYC expression in *MLL*-r B-ALL cells (Figure 4J). Following transduction and sorting of GFP^+ B-ALL PDX cells, culture in the presence of doxycycline for 14 days preserved $CD34^+$ content (Figure 4K). Together, these data suggest that MYC promotes the reconstitution of *MLL*-r B-ALL from $CD34^-$ cells.

Inhibition of oxidative metabolism promotes emergence of primitive LICs

Our transcriptional profiling suggested that engrafting *MLL*-r B-ALL cells are metabolically heterogeneous, with 34−r cells recruiting latent LIC properties possibly through activating oxidative phosphorylation to engraft and reconstitute the B-ALL cellular diversity (Figure 4C). We hypothesized that, by targeting oxidative phosphorylation, we could impede emergence of LICs from 34− blasts. This hypothesis is supported by findings in AML, where LICs have been reported to depend on mitochondrial oxidative phosphorylation (Jones et al., 2018; Lagadinou et al., 2013). Using the Mitotracker dye to quantify mitochondrial content in *MLL*-r B-ALL cells, we confirmed that 34−r cells contained a higher level of mitochondrial content compared with bulk cells, with a trend toward higher mitochondrial numbers (Figures 5A, 5B, S5B, and S5C). Using the Seahorse Mito Stress assay, we observed that 34−r cells possessed higher rates of mitochondrial respiration compared with steady-state *MLL*-r B-ALL blasts (Figures 5C and 5D). We found that MYC activity modulated mitochondrial metabolism in *MLL*-r cells using both

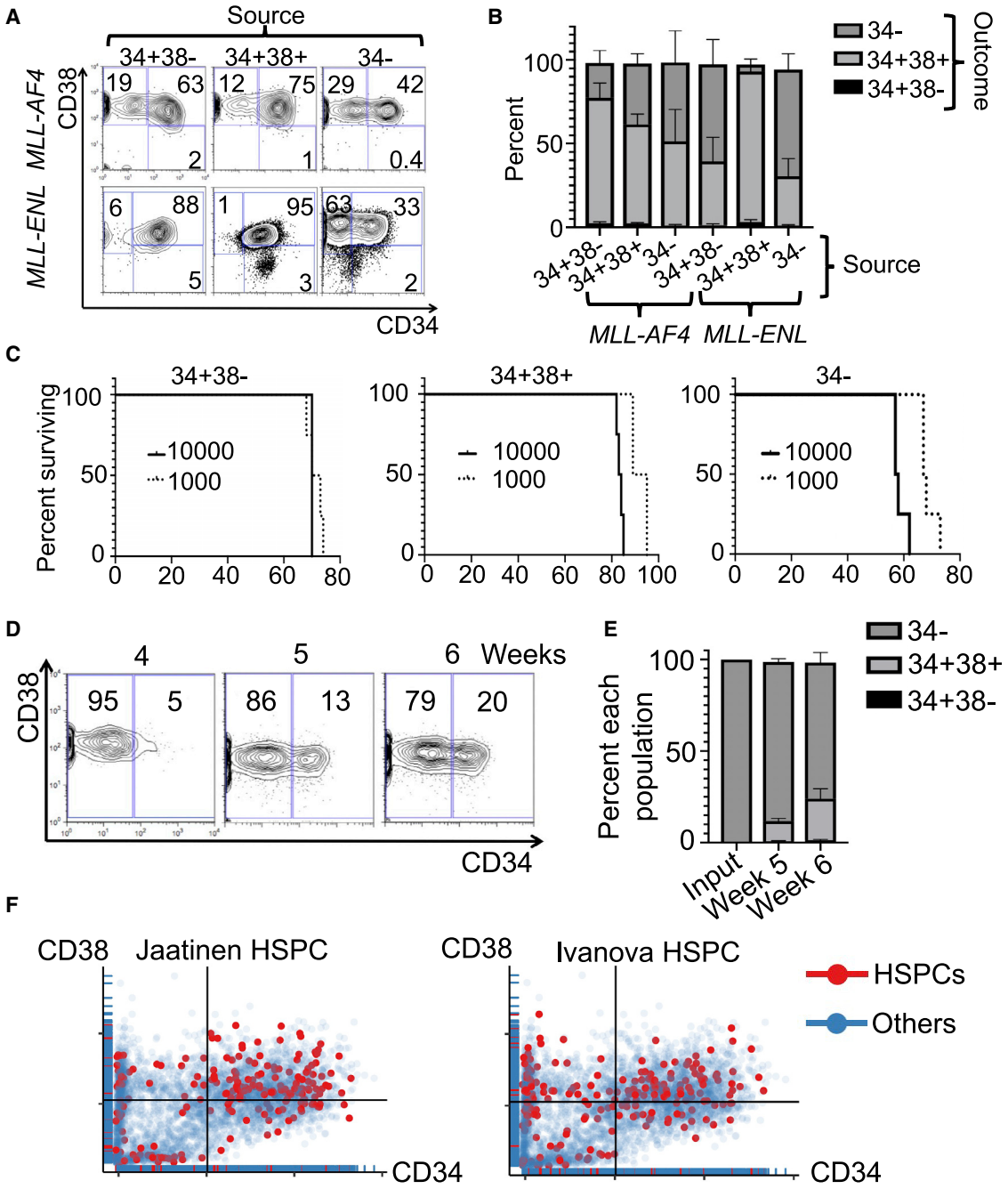

Figure 3. LIC emergence from all hierarchical levels

(A) Representative flow cytometry profiles of terminal leukemias derived from the indicated transplanted cell populations gated on viable and human CD45$^+$ cells within the bone marrow.

(B) Proportions of each cell type in outcome leukemias derived from the indicated transplanted cell sources are presented (p = NS by ANOVA comparing each outcome population between leukemia sources except in *MLL-ENL* leukemia, where $p < 0.05$ comparing the 34+38+ and 34− outcomes of leukemias derived from 34+38+ to both 34+38− and 34− derived leukemia).

(C) Terminal leukemias derived from the indicated cell populations of *MLL-AF4* primary transplants were transplanted into secondary recipients at the indicated doses and the onset of terminal leukemia monitored.

(D and E) 34− cells were purified from *MLL-AF4* leukemia and transplanted into recipient mice. Reconstitution of CD34$^+$ populations was quantified over time.

(F) CITE-seq was performed on *MLL-AF4* leukemia. Cells were scored for enrichment of HSPC signatures (signature score above 95th percentile cutoff defining "HSPC") and plotted versus CD34 and CD38 expression determined from barcoded antibodies (Ivanova et al., 2002; Jaatinen et al., 2006). In all experiments, results are presented as mean ± SEM and results compared by Student's t test, with p value shown.

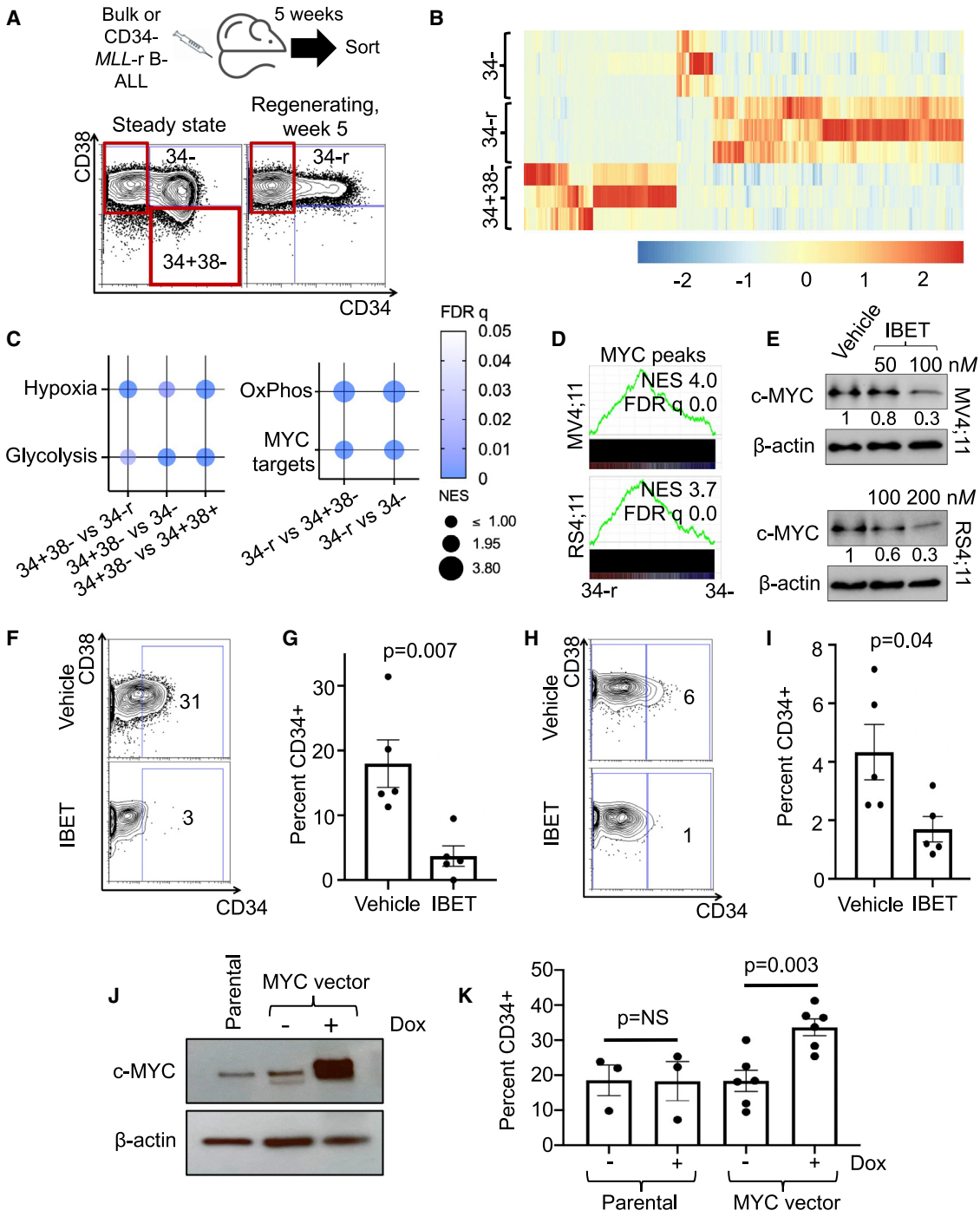

Figure 4. MYC regulates *MLL*-r B-ALL LIC state

(A) Schematic showing the input populations sorted for RNA-seq, including 34+38− cells and 34− cells steady state (left) and from regenerating 34− cells (right) in mouse bone marrow.

(B) RNA-seq was performed on the indicated FACS-sorted populations and differential gene expression analyzed (cutoff $\log_2$ fold change > 0.5 and $p_{adj} < 0.05$).

(C) Gene set enrichment analysis (GSEA) was used to identify differentially enriched signatures (circle size indicates normalized enrichment score [NES] with shading representing false discovery rate [FDR] q value).

(D) MYC ChIP-seq was performed in MV4;11 and RS4;11 cells and peaks associated with transcriptional start sites identified. GSEA was performed using preranked lists comparing transcript expression of 34−r versus 34− cells.

(E) MV4;11 or RS4;11 cells were treated for 48 h with the indicated concentrations of IBET-151, at which time MYC protein was measured by western blot with bands quantified (relative to β-actin).

(legend continued on next page)

IBET-151 and the direct MYC inhibitor KI-MS2-008 (MS2) (Figures S5D–S5T; Struntz et al., 2019). To determine whether targeting oxidative metabolism affected reconstitution of *MLL*-r B-ALL, we used tigecycline, an inhibitor of mitochondrial translation, which has been advanced as a candidate therapy targeting LICs in AML and chronic myeloid leukemia (Kuntz et al., 2017; Skrtic et al., 2011). We found that tigecycline decreased viability of *MLL*-r B-ALL cells in culture and diminished mitochondrial content (Figures S5U–S5X). We next treated 34− cells reconstituting *in vivo* with a course of tigecycline starting at 3 weeks post-engraftment, when we would expect the reconstitution process to commence (Figure 3D). We found that this decreased overall disease burden (Figures 5E–5H). However, at completion of the treatment course, tigecycline promoted emergence of $CD34^+$ cells, suggestive of induction of an LIC-enriched state (Figures 5I and 5J). We found that, despite the early effect of tigecycline on chimerism, there was no benefit in survival studies (Figures 5K and 5L). Secondary transplantation of vehicle- or tigecycline-treated leukemia confirmed that tigecycline treatment promoted LIC emergence from 34− cells *in vivo* (Figure 5M). These findings indicate that inhibition of oxidative phosphorylation could enforce an LIC-enriched state and that oxidative phosphorylation is not an LIC dependency.

34+38− B-ALL LICs maintain a glycolytic state

Since blockade of mitochondrial translation facilitates LIC emergence, this further supported the notion that *MLL*-r B-ALL LICs maintain a relative glycolytic state. Indeed, we observed that treatment of *MLL*-r B-ALL cells with tigecycline not only decreased the oxygen consumption rate (OCR) but also the OCR/extracellular acidification rate (ECAR) ratio, consistent with a shift toward glycolysis (Figures 6A–6C; Potter et al., 2016). Therefore, we next sought to better understand the energy state of 34+38− LIC-enriched cells. 34+38− cells showed lower levels of reactive oxygen species and mitochondrial content compared with 34− cells (Figures 6D–6F, S6A, and S6B). *Ex vivo* culture of *MLL*-r B-ALL cells under hypoxic conditions preserved the 34+38− state more effectively than normoxic culture (Figure 6G). By analyzing our ChIP-seq data, we found that MYC-bound peaks were enriched in gene ontology terms related to both oxidative phosphorylation and the hypoxic response and that MYC directly bound key glycolysis-associated loci (Figures 6H and 6I; Fang et al., 2019). We did not observe consistent enrichment of HIF-1α protein in 34+38− cells, suggesting that the relative dependence on glycolysis is due to lower levels of oxidative phosphorylation (Figure S6C). Consistent with this, in an independent dataset, we observed that predicted corticosteroid-resistant LICs showed a lower oxidative phosphorylation signature (Candelli et al., 2022; Figure S6D). Inhibiting MYC with IBET-151 impaired glycolytic activity in MV4;11 cells (Figures 6J and 6K). Together, these data indicate that the LIC-enriched 34+38− fraction maintains a relative MYC-maintained glycolytic state.

Inhibiting hypoxic glycolysis to target *MLL*-r B-ALL LICs

Inhibition of glycolysis has been pursued as an approach to cancer therapy as a means of targeting the Warburg effect, and so we next examined glycolysis as a target in *MLL*-r B-ALL. Dichloroacetate (DCA) is an inhibitor of pyruvate dehydrogenase kinase that shunts pyruvate into the tricarboxylic acid (TCA) cycle and away from lactate production (Bonnet et al., 2007). As expected, DCA increased oxidative metabolism in MV4;11 cells and *MLL*-r B-ALL PDX cells (Figures S6E–S6H). Treatment of MV4;11 cells with either DCA or the direct glycolysis inhibitor 3-BP diminished leukemic progenitor cells in colony formation assays (Figures S6I). DCA decreased the viability of B-ALL cells selectively under hypoxic conditions, where cells would be more reliant on glycolysis (Figure S6J). Treatment of mice xenografted with 34+38− B-ALL cells with DCA resulted in a modest but significant survival benefit (Figure S6K).

Since glycolysis is preferentially utilized under hypoxic conditions, we treated *MLL*-r cell lines and xenografts with the HIF-1α inhibitor echinomycin (Wang et al., 2011). Echinomycin treatment decreased the viability of a panel of human *MLL*-r B-ALL specimens while relatively preserving healthy human HSPCs, suggestive of a degree of HIF-1α dependence in all blasts (Figures 7A and S6L). Echinomycin treatment ablated the viability and colony forming capacity of MV4;11 cells and the viability of RS4;11 cells at low nM concentrations (Figures 7B and 7C). Moreover, we found that echinomycin treatment impaired leukemic progenitors in a mouse model of *MLL-AF9*-driven mixed B-lymphoid and myeloid leukemia (Figure S6M; Rowe et al., 2019). We found that, following 2 weeks of echinomycin treatment, mice bearing *MLL*-r B-ALL xenografts showed diminished overall disease burden as well as $CD34^+$ content *in vivo* (Figures 7D–7F). By monitoring for survival following an upfront 2-week treatment course, we found that echinomycin prolonged survival of mice bearing B-ALL xenografts (Figure 7G). Secondary transplantation indicated LIC depletion (Figure 7H). Finally, we tested the potential of combined treatment with echinomycin and DCA, finding that this combination promoted survival (Figures 7I and S6N). Echinomycin did not cause overt toxicity and effected only subtle changes on hematologic parameters, with myeloid skewing observed in the peripheral blood and at the HSPC level (Figures S6O and S6P). Together, these findings indicate the feasibility of inhibiting glycolysis and hypoxic signaling as a means of targeting LICs in B-ALL.

(F and G) FACS-sorted $CD34^-$ cells were cultured on MS5 stroma for 14 days with DMSO vehicle or 50 nM IBET-151, at which time the $CD34^+$ content of the cultures was quantified (n = 5 independent donors).
(H and I) CD34−r cells were engrafted into NSG mice for 3 weeks, at which time a 2-week treatment course with IBET-151 began, after which the human $CD45^+$ content of the bone marrow was analyzed by flow cytometry with the indicated markers (n = 5 mice per group).
(J) K562 cells were transduced with a doxycycline-inducible MYC vector and treated with or without doxycycline for 72 h, at which time MYC levels were measured by western blotting.
(K) *MLL*-r B-ALL cells were transduced or not transduced with the doxycycline-inducible MYC vector, sorted for GFP^+ cells, and cultured on MS5 stroma with cytokines with or without doxycycline for 14 days, at which time $CD34^+$ content of the cultures was measured by flow cytometry. NS, not significant.
In all experiments, results are presented as mean ± SEM and results compared by Student's t test, with p value shown.

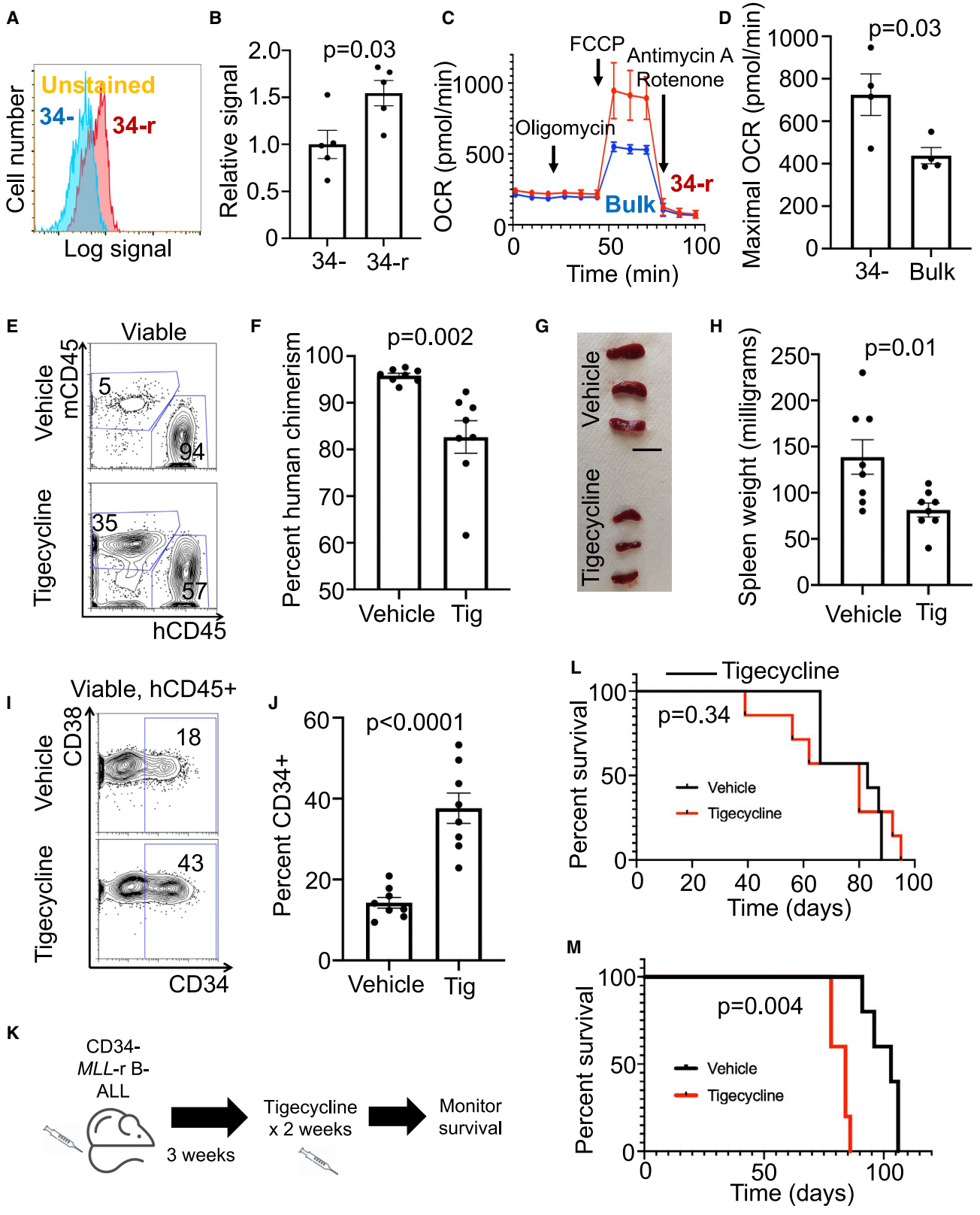

(legend on next page)

DISCUSSION

In this study, we aimed to gain understanding of LIC biology using LIC-rich, human B-lymphoid and myeloid multipotent *MLL*-r B-ALL as a model. Although the heterogeneous cells of *MLL*-r B-ALL appear to follow a hierarchical organization, in that LICs are enriched in the most undifferentiated fraction, engraftable, self-renewing cells emerge from all levels of this hierarchy. We find that LICs in *MLL*-r B-ALL bear hallmarks of cancer stem cells—some of which were until recently thought to be specific to solid tumors—including cell state plasticity (Gupta et al., 2019; Jones et al., 2018; Lee et al., 2017). Our findings uncover aspects of the biology underlying the aggressive clinical behavior of this high-risk form of B-ALL.

Since the initial supposition of LICs, models of leukemic ontogeny have been built upon paradigms of normal hematopoiesis (Bonnet and Dick, 1997; Kreso and Dick, 2014; Pollyea and Jordan, 2017). Based on seminal studies performed in AML, the "classic" conclusions that LICs are both uniform and rare akin to normal HSCs have gradually been revised (Pollyea and Jordan, 2017). At first glance, our data would appear to be consistent with this classic model in that we found distinct populations stratified from least to most primitive based on transcriptional profiles, immunophenotypes, and engraftment capacities. In B-ALL, though engrafting LICs have been reported in multiple populations, suggestive of a stochastic rather than hierarchical organization, their relative frequency in each of these apparent differentiation states has not previously been quantified (Prieto et al., 2018; Aoki et al., 2015; Bardini et al., 2015; Kong et al., 2008; Lapidot et al., 1994; le Viseur et al., 2008). Our findings indicate that LICs are quantitatively enriched in relatively dedifferentiated fractions but can also emerge from more differentiated fractions, accounting for this apparent stochasticity (Elder et al., 2017). Use of more immunodeficient mouse models with heightened sensitivity for human engraftment has suggested plasticity of AML cells like our findings, although the molecular mechanisms underpinning this effect were unclear (Ng et al., 2016; Sarry et al., 2011). The consensus is emerging that, across many forms of leukemia, leukemic ontogeny departs from the strict stratification and unidirectional differentiation of healthy hematopoiesis and that LICs are not uniform in their marker profiles (Ng et al., 2016). Despite LIC paradigms undergoing revision, the notion that engraftable LIC content predicts disease outcome highlights the importance of LICs in leukemic pathobiology and provides an ongoing impetus for investigation of the determinants of their state (Monaco et al., 2004; Paczulla et al., 2017). Our findings expand understanding of B-ALL LICs by demonstrating latency in phenotypically mature (i.e., 34−) populations in addition to the known genetic and immunophenotypic heterogeneity (Anderson et al., 2011; Aoki et al., 2015).

Our data reinforce the idea that LIC identity can be fluid, as has been described in stem cells of solid tumors and sporadically in LICs (Fumagalli et al., 2020; Gupta et al., 2019). Use of NSG mice led to the evidence that AML LICs within $CD34^-$ fractions could reconstitute the full cellular diversity of the original AML specimen, although the mechanism of this cell state interconversion was unknown (Sarry et al., 2011). A recent study reported that acute promyelocytic leukemia cells undergoing differentiation driven by retinoic acid could re-acquire the LIC state following drug withdrawal (McKenzie et al., 2019). In B-ALL, we detected LIC emergence from all immunophenotypic populations—even the least primitive $CD34^-$ blasts—with the capability of reconstituting the full cellular diversity of the original leukemia. These findings are likely relevant to alterations in the LIC state occurring as an adaptation to therapy at relapse of B-ALL (Dobson et al., 2020).

Our efforts to uncover determinants of the LIC state led us to MYC signaling. Oncogenic MYC activity is a downstream effector of transforming MLL translocations, and mitochondrial turnover is important for LIC homeostasis (Dawson et al., 2011; Pei et al., 2018). MYC can drive both mitochondrial oxidative metabolism and glycolysis in cancer (Fang et al., 2019; Lee et al., 2017). We impaired MYC activity, finding that this intervention perturbed cellular metabolism and blocked the conversion of $CD34^-$ to $CD34^+$ cells (Bardini et al., 2018; Dawson et al., 2011; Delmore et al., 2011). Although we found that direct inhibition of mitochondrial translation transiently impeded growth of cells *in vivo*, this intervention promoted the emergence of $CD34^+$ cells enriched in engrafting LICs, suggesting that inhibition of oxidative phosphorylation facilitates transition to the quiescent, glycolytic LIC state. Our data indicate that LICs are quiescent and glycolytic with low levels of oxidative phosphorylation and reactive oxygen species compared with other populations. In AML, LICs also contain relatively low levels of reactive oxygen species; however, in contrast to our findings, AML LICs seem to have low glycolytic reserve and are therefore susceptible to inhibition of oxidative phosphorylation (Jones et al., 2018; Lagadinou et al., 2013). The metabolic state of *MLL*-r B-ALL LICs seems to be co-opted from normal long-term HSCs and could explain the concomitant retention of

Figure 5. Targeting oxidative phosphorylation drives LIC emergence

(A and B) Active mitochondria were quantified in bulk leukemia or 34−r cells using Mitotracker green, with representative flow cytometry results presented compared with background of unstained cells (n = 5 biologic replicates each over two independent experiments).

(C and D) The indicated B-ALL cell populations were cultured on MS5 stroma for 72 h prior to analysis of oxygen consumption rate (OCR) by Seahorse Mito Stress Assay (results normalized to 10^6 viable cells and aggregated over two independent experiments, four biologic replicates each).

(E and F) NSG mice were engrafted with *MLL*-r B-ALL for 3 weeks, at which time treatment with tigecycline commenced and continued for 2 weeks, when the mice were euthanized and mouse and human chimerism within the bone marrow analyzed (n = 8 subjects in vehicle and tigecycline groups).

(G and H) Spleens were isolated and weighed at the endpoint from (C) (scale bar represents 1 cm).

(I and J) $CD34^+$ content of the xenografts isolated in (E) was analyzed by flow cytometry (n = 8 subjects in vehicle and tigecycline groups).

(K and L) Xenotransplanted NSG mice were treated with the same course of tigecycline as in (E) but followed to the onset of terminal leukemia (n = 7 subjects in vehicle and tigecycline groups; survival compared with log rank test).

(M) NSG mice were secondarily transplanted with primary grafts from (E) and survival compared by log rank test (n = 5 subjects in each group).

In all experiments, unless otherwise stated, results are presented as mean ± SEM and results compared by Student's t test, with p value shown.

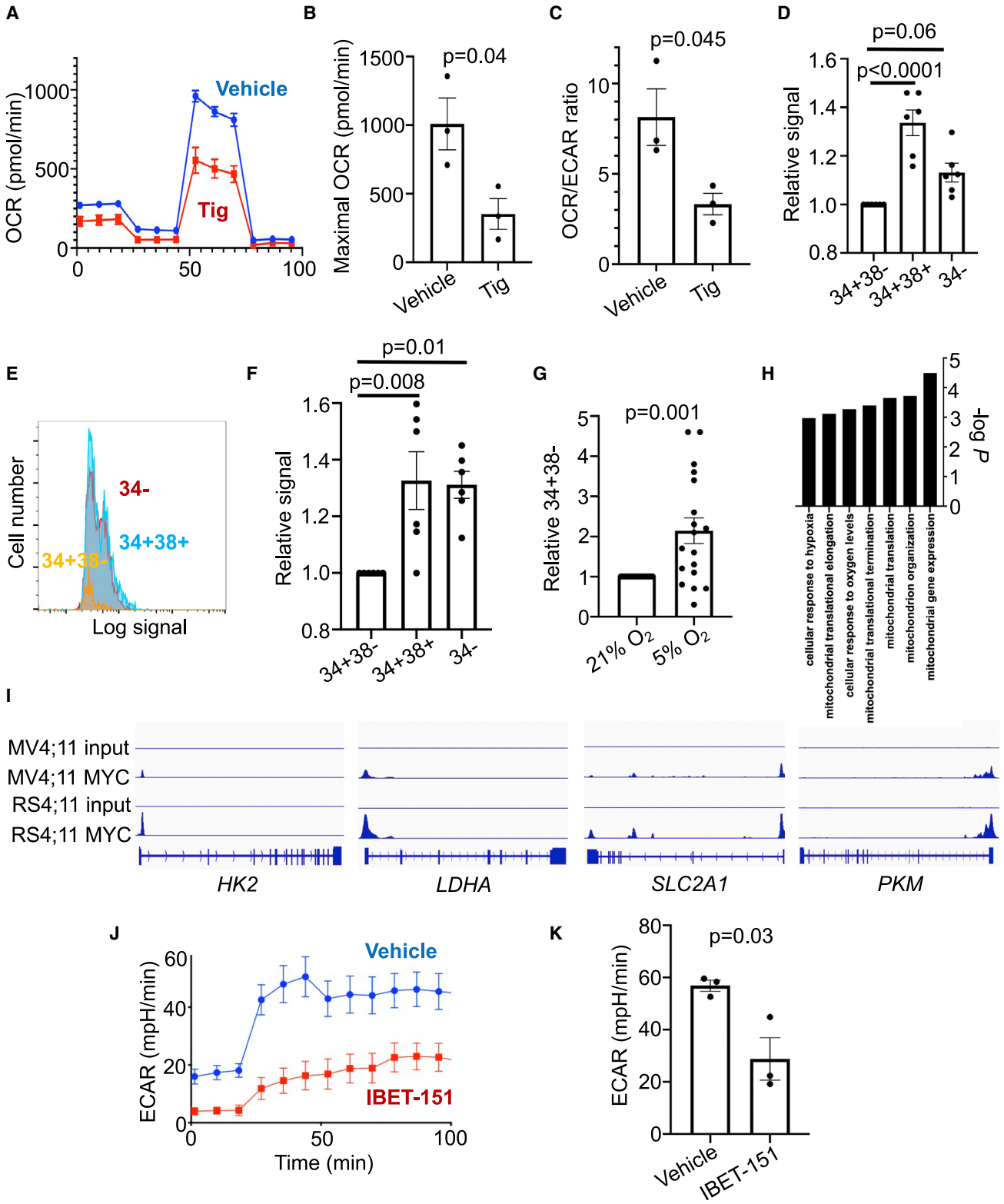

Figure 6. Primitive *MLL*-r B-ALL LICs maintain a glycolytic state

(A–C) Human *MLL*-r B-ALL cells were cultured in the presence of vehicle or tigecycline (1 μM) for 72 h, at which time OCR and ECAR were measured by Seahorse assay (results aggregated over three biologic replicates).

(legend continued on next page)

multipotency programs in this form of leukemia (Nakamura-Ishizu et al., 2020; Qiu et al., 2021; Spencer et al., 2014; Takubo et al., 2010). MYC seems to fulfill context-specific roles in B-ALL cells both as an activator of oxidative phosphorylation to promote leukemic reconstitution by 34− blasts as well as to maintain glycolysis to support the primitive LIC state. Although *MLL*-r B-ALL typically contains relatively few somatic mutations, future study will investigate the role of clonal heterogeneity and DNA methylation alterations in establishing LIC ontogeny (Andersson et al., 2015; Tejedor et al., 2021).

Our conclusion that the latent LICs can emerge from relatively differentiated blasts can be connected to the clinical behavior of this form of high-risk B-ALL and may have therapeutic implications. We find latent myeloid transdifferentiation potential within single-cell-derived clones from each stratum of the leukemic hierarchy, consistent with a multipotent cell state (Rossi et al., 2012). The coexisting LIC and lineage plasticity in *MLL*-r B-ALL provides two distinct mechanisms of chemotherapy evasion. We conclude that the high functional LIC content and plasticity in both lineage and the LIC state likely contribute to the poor outcomes of *MLL*-r B-ALL (Pieters et al., 2019). Our approach to understanding the mechanisms of LIC variation uncovered glycolysis as a potential vulnerability in *MLL*-r B-ALL. A recent report used scRNA-seq to characterize corticosteroid-resistant, putative relapse-initiating cells, confirming that these cells seemed to be largely quiescent (Candelli et al., 2022). Better understanding of the molecular basis of LICs in other forms of leukemia relative to normal hematopoiesis could lead to candidate therapies.

Overall, we show that LICs in high-risk B-ALL (1) maintain an HSC- and MPP-like state and retain multipotency programs; (2) are frequent compared with reported LIC frequencies in AML; (3) are relatively glycolytic, with the LIC state implemented upon inhibition of oxidative phosphorylation, contrasting with dependency of LICs on oxidative phosphorylation in myeloid leukemias (Kuntz et al., 2017; Lagadinou et al., 2013; Skrtic et al., 2011); and (4) the glycolytic state of *MLL*-r B-ALL LICs is a therapeutic vulnerability. Our findings in *MLL*-r B-ALL reinforce the notion that LICs are adaptable, providing possible explanations as to why therapies targeting LICs have yet to prove widespread efficacy despite being the object of intense investigation for over 2 decades (Pollyea and Jordan, 2017; Saygin et al., 2019). Our data would suggest that a hybrid hierarchical and stochastic LIC ontogeny exists in *MLL*-r B-ALL, with a highly engraftable population detected but considerable flux through all populations likely manifesting as stochasticity seen in prior studies and, to a degree, in our transplants (Aoki et al., 2015; le Viseur et al., 2008). Further studies will determine the relative cell-intrinsic and extrinsic contributions to the relatively glycolytic LIC state in B-ALL, as well as the mechanisms relating metabolism and stemness in B-ALL, which remain elusive (Hayashi et al., 2018).

Limitations of the study

Our study was performed using human-patient-derived leukemia cells, which provides translational relevance compared with studies reliant exclusively on inbred mouse models. However, this human system comes with the limitation that only relatively few donor specimens could be used for quantitative xenotransplantation and in-depth analysis of LIC function (seven used in this study), with inter-patient variability challenging to mitigate using such a design. Our use of FACS-sorted populations in xenotransplantation assays could confound results due to incomplete purity, in particular underestimating differences in LIC content between populations, though we aimed to mitigate this using single-cell-level studies. We also narrowed our focus to *MLL*-r B-ALL, raising the questions as to generalizability to other forms of high-risk B-ALL. Indeed, our analysis of *BCR-ABL*-driven B-ALL would suggest alternative LIC ontogeny that should be investigated in future study.

STAR★METHODS

Detailed methods are provided in the online version of this paper and include the following:

- KEY RESOURCES TABLE
- RESOURCE AVAILABILITY
  - Lead contact
  - Materials availability
  - Data and code availability
- EXPERIMENTAL MODEL AND SUBJECT DETAILS
  - Animal models
  - Human subjects
  - Cell culture
- METHOD DETAILS
  - Flow cytometry and cell sorting
  - Morphology
  - Recombinant DNA
  - Western blotting
  - Seahorse Mito Stress assay
  - Long-term culture initiating cell assay

(D) Relative Mitotracker signal was quantified in the indicated populations from two independent leukemia sources (n = 6 biologic replicates over two experiments compared by one-way ANOVA with p values shown).
(E and F) CellRox was used to stain for reactive oxygen species in *MLL*-r B-ALL cells and relative signal quantified (n = 6 biologic replicates comparisons by ANOVA with p values shown).
(G) PDX cells were cultured for 10 days under either 21% oxygen or 5% oxygen, and the composition of the cultures was measured by flow cytometry (result combined across three independent experiments).
(H) Gene ontology analysis was used to query for terms enriched in MYC ChIP-seq peaks in RS4;11 cells.
(I) Visualization of MYC ChIP-seq peaks associated with the indicated glycolytic genes in MV4;11 and RS4;11, with control input for each shown.
(J and K) MV4;11 cells were cultured in the presence or absence of 50 nM IBET-151 for 72 h, at which time the extracellular acidification rate (ECAR) was measured using the Seahorse assay.
Unless otherwise indicated, in all experiments, results are presented as mean ± SEM and results compared by Student's t test, with p value shown.

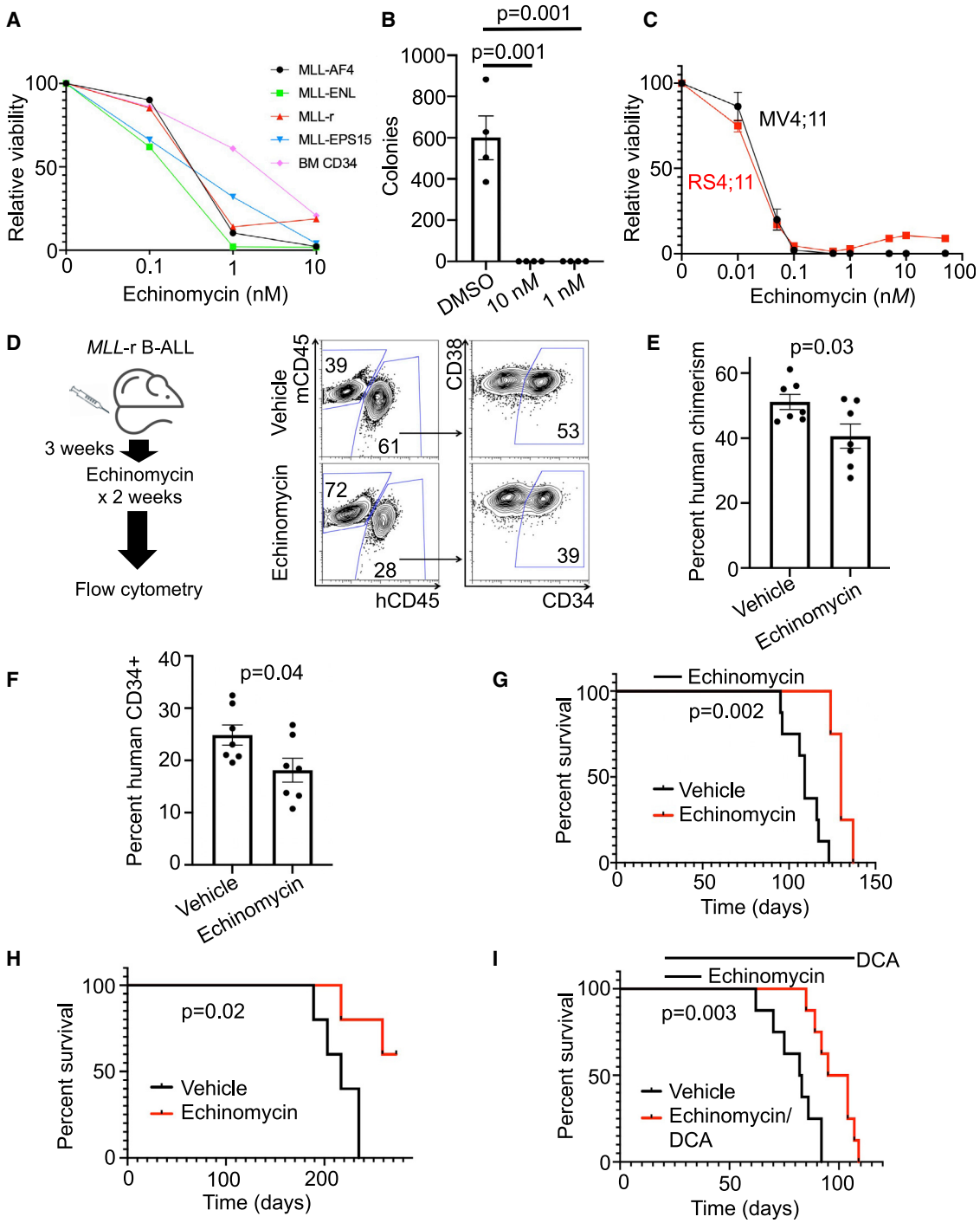

Figure 7. Targeting glycolysis and hypoxic signaling

(A) The indicated *MLL*-r B-ALL specimens or normal human bone marrow (BM) CD34$^+$ HSPCs were cultured in the presence of the indicated concentrations of echinomycin for 72 h, at which time cell viability was quantified.

(B) One thousand MV4;11 cells were cultured in the presence or absence of the indicated concentrations of echinomycin for 48 h and then placed in methylcellulose culture. After 5 days, colony formation was quantified (compared by t test with p values shown).

(C) MV4;11 or RS4;11 cells were cultured with the indicated concentration of echinomycin for 48 h, at which time viability was measured (n = 3 independent experiments).

(D–F) NSG mice were transplanted with *MLL-AF4* B-ALL cells. Three weeks following engraftment, mice were treated with echinomycin for 2 weeks, at which time human CD45 and CD34 chimerism were analyzed.

(legend continued on next page)

- Reverse transcription PCR
- Single cell RNA sequencing
- Bulk RNA sequencing library preparation
- Data analysis
- ChIP-seq

- QUANTIFICATION AND STATISTICAL ANALYSIS

SUPPLEMENTAL INFORMATION

Supplemental information can be found online at https://doi.org/10.1016/j.celrep.2022.110752.

ACKNOWLEDGMENTS

The authors thank the Single Cell Core at Harvard Medical School, Boston, MA for performing the single-cell RNA-seq sample preparation. We thank the Molecular Biology Core Facility at the Dana-Farber Cancer Institute for sequencing studies. We thank William Oldham at the Seahorse Core at Brigham and Women's Hospital. We thank the Flow Cytometry Core at Boston Children's Hospital. This work was supported by the National Institute of Diabetes and Digestive and Kidney Diseases (K08 DK114527 to R.G.R.) as well as grants from the St. Baldrick's Foundation, Pablove Foundation, Department of Defense (CA201001), and Pedals for Pediatrics (to R.G.R.); the National Heart, Lung, Blood Institute (U01 HL134812 to G.Q.D.); the National Center for Advancing Translational Sciences (UL 1TR002541 to S.H.S.); the Harvard Medical School Foundry (to S.H.S.); the Leukemia and Lymphoma Society of America (to G.Q.D.); and the Coordination for the Improvement of Higher Education Personnel (CAPES/Brazil) (to E.L.d.R. and R.V.d.S.). We thank Scott Armstrong for helpful discussions.

AUTHOR CONTRIBUTIONS

Conceptualization, R.G.R. and E.L.d.R.; methodology, R.G.R. and E.L.d.R.; software, E.L.d.R.; formal analysis, J.K., S.H.S., S.N., R.G.R., and E.L.d.R.; investigation, V.M., D.W., Z.L., T. Hughes, E.L.d.R., M.F., R.V.d.S., T.C., P. Sousa, P. Schneider, T.M., F.C.P.H., W.M., T. Harada, P. Sensharma, and R.G.R.; resources, Y.P., M.H., A.N.K., and A.K.S.; data curation, R.G.R., M.P., T. Hughes, and E.L.d.R.; writing – original draft, R.G.R. and E.L.d.R.; writing – revising and editing, A.K.S., T.E.N., M.P., and R.G.R.; supervision, T.E.N., M.P., R.W.S., S.H.O., G.Q.D., M.P., and R.G.R.; project administration, T.E.N., G.Q.D., and R.G.R.; funding acquisition, G.Q.D. and R.G.R.

DECLARATION OF INTERESTS

G.Q.D. holds equity in companies pursuing anti-cancer treatments (including Epizyme and 28-7 Therapeutics) and patents related to cancer therapeutics. A.K.S. reports compensation for consulting and/or science advisory board (SAB) membership from Merck, Honeycomb Biotechnologies, Cellarity, Repertoire Immune Medicines, Ochre Bio, Third Rock Ventures, Hovione, Relation Therapeutics Limited, Empress Therapeutics, FL82, and Dahlia Biosciences.

Received: October 13, 2021
Revised: January 24, 2022
Accepted: April 7, 2022
Published: April 26, 2022

REFERENCES

Anderson, K., Lutz, C., van Delft, F.W., Bateman, C.M., Guo, Y., Colman, S.M., Kempski, H., Moorman, A.V., Titley, I., Swansbury, J., et al. (2011). Genetic variegation of clonal architecture and propagating cells in leukaemia. Nature *469*, 356–361.

Andersson, A.K., Ma, J., Wang, J., Chen, X., Gedman, A.L., Dang, J., Nakitandwe, J., Holmfeldt, L., Parker, M., Easton, J., et al. (2015). The landscape of somatic mutations in infant MLL-rearranged acute lymphoblastic leukemias. Nat. Genet. *47*, 330–337.

Aoki, Y., Watanabe, T., Saito, Y., Kuroki, Y., Hijikata, A., Takagi, M., Tomizawa, D., Eguchi, M., Eguchi-Ishimae, M., Kaneko, A., et al. (2015). Identification of CD34+ and CD34- leukemia-initiating cells in MLL-rearranged human acute lymphoblastic leukemia. Blood *125*, 967–980.

Bardini, M., Trentin, L., Rizzo, F., Vieri, M., Savino, A.M., Garrido Castro, P., Fazio, G., Van Roon, E.H.J., Kerstjens, M., Smithers, N., et al. (2018). Antileukemic efficacy of BET inhibitor in a preclinical mouse model of MLL-AF4(+) infant ALL. Mol. Cancer Ther. *17*, 1705–1716.

Bardini, M., Woll, P.S., Corral, L., Luc, S., Wittmann, L., Ma, Z., Lo Nigro, L., Basso, G., Biondi, A., Cazzaniga, G., et al. (2015). Clonal variegation and dynamic competition of leukemia-initiating cells in infant acute lymphoblastic leukemia with MLL rearrangement. Leukemia *29*, 38–50.

Boissel, N., and Baruchel, A. (2018). Acute lymphoblastic leukemia in adolescent and young adults: treat as adults or as children? Blood *132*, 351–361.

Bonnet, D., and Dick, J.E. (1997). Human acute myeloid leukemia is organized as a hierarchy that originates from a primitive hematopoietic cell. Nat. Med. *3*, 730–737.

Bonnet, S., Archer, S.L., Allalunis-Turner, J., Haromy, A., Beaulieu, C., Thompson, R., Lee, C.T., Lopaschuk, G.D., Puttagunta, L., Bonnet, S., et al. (2007). A mitochondria-K+ channel axis is suppressed in cancer and its normalization promotes apoptosis and inhibits cancer growth. Cancer Cell *11*, 37–51.

Candelli, T., Schneider, P., Garrido Castro, P., Jones, L.A., Bodewes, E., Rockx-Brouwer, D., Pieters, R., Holstege, F.C.P., Margaritis, T., and Stam, R.W. (2022). Identification and characterization of relapse-initiating cells in MLL-rearranged infant ALL by single-cell transcriptomics. Leukemia *36*, 58–67.

Chapuy, B., McKeown, M.R., Lin, C.Y., Monti, S., Roemer, M.G., Qi, J., Rahl, P.B., Sun, H.H., Yeda, K.T., Doench, J.G., et al. (2013). Discovery and characterization of super-enhancer-associated dependencies in diffuse large B cell lymphoma. Cancer Cell *24*, 777–790.

Chen, C., Yu, W., Alikarami, F., Qiu, Q., Chen, C.H., Flournoy, J., Gao, P., Uzun, Y., Fang, L., Davenport, J.W., et al. (2021). Single-cell multiomics reveals increased plasticity, resistant populations and stem-cell-like blasts in KMT2A-rearranged leukemia. Blood *139*, 2198–2211.

Dawson, M.A., Prinjha, R.K., Dittmann, A., Giotopoulos, G., Bantscheff, M., Chan, W.I., Robson, S.C., Chung, C.W., Hopf, C., Savitski, M.M., et al. (2011). Inhibition of BET recruitment to chromatin as an effective treatment for MLL-fusion leukaemia. Nature *478*, 529–533.

de Almeida, M.J., Luchsinger, L.L., Corrigan, D.J., Williams, L.J., and Snoeck, H.W. (2017). Dye-independent methods reveal elevated mitochondrial mass in hematopoietic stem cells. Cell Stem Cell *21*, 725–729.e4.

Delmore, J.E., Issa, G.C., Lemieux, M.E., Rahl, P.B., Shi, J., Jacobs, H.M., Kastritis, E., Gilpatrick, T., Paranal, R.M., Qi, J., et al. (2011). BET bromodomain inhibition as a therapeutic strategy to target c-Myc. Cell *146*, 904–917.

Dobson, S.M., Garcia-Prat, L., Vanner, R.J., Wintersinger, J., Waanders, E., Gu, Z., McLeod, J., Gan, O.I., Grandal, I., Payne-Turner, D., et al. (2020).

(G) Mice xenotransplanted with *MLL-AF4* B-ALL were treated for 2 weeks with echinomycin or vehicle (treatment window indicated) and survival monitored following completion of treatment.
(H) Cells from mice in (G) were secondarily transplanted and survival of recipient mice monitored.
(I) Mice xenotransplanted with *MLL-AF4* leukemia were treated for echinomycin or vehicle for 2 weeks and then with or without DCA and survival monitored.
In all experiments, unless otherwise stated, results are presented as mean ± SEM and results compared by Student's t test or log rank test for survival analysis, with p value shown.

Relapse-fated latent diagnosis subclones in acute B lineage leukemia are drug tolerant and possess distinct metabolic programs. Cancer Discov. *10*, 568–587.

Doulatov, S., Notta, F., Eppert, K., Nguyen, L.T., Ohashi, P.S., and Dick, J.E. (2010). Revised map of the human progenitor hierarchy shows the origin of macrophages and dendritic cells in early lymphoid development. Nat. Immunol. *11*, 585–593.

Elder, A., Bomken, S., Wilson, I., Blair, H.J., Cockell, S., Ponthan, F., Dormon, K., Pal, D., Heidenreich, O., and Vormoor, J. (2017). Abundant and equipotent founder cells establish and maintain acute lymphoblastic leukaemia. Leukemia *31*, 2577–2586.

Fang, Y., Shen, Z.Y., Zhan, Y.Z., Feng, X.C., Chen, K.L., Li, Y.S., Deng, H.J., Pan, S.M., Wu, D.H., and Ding, Y. (2019). CD36 inhibits beta-catenin/c-myc-mediated glycolysis through ubiquitination of GPC4 to repress colorectal tumorigenesis. Nat. Commun. *10*, 3981.

Fumagalli, A., Oost, K.C., Kester, L., Morgner, J., Bornes, L., Bruens, L., Spaargaren, L., Azkanaz, M., Schelfhorst, T., Beerling, E., et al. (2020). Plasticity of Lgr5-negative cancer cells drives metastasis in colorectal cancer. Cell Stem Cell *26*, 569–578.

Gierahn, T.M., Wadsworth, M.H., 2nd, Hughes, T.K., Bryson, B.D., Butler, A., Satija, R., Fortune, S., Love, J.C., and Shalek, A.K. (2017). Seq-well: portable, low-cost RNA sequencing of single cells at high throughput. Nat. Methods *14*, 395–398.

Guan, Y., Gerhard, B., and Hogge, D.E. (2003). Detection, isolation, and stimulation of quiescent primitive leukemic progenitor cells from patients with acute myeloid leukemia (AML). Blood *101*, 3142–3149.

Gupta, P.B., Pastushenko, I., Skibinski, A., Blanpain, C., and Kuperwasser, C. (2019). Phenotypic plasticity: driver of cancer initiation, progression, and therapy resistance. Cell Stem Cell *24*, 65–78.

Hayashi, Y., Zhang, Y., Yokota, A., Yan, X., Liu, J., Choi, K., Li, B., Sashida, G., Peng, Y., Xu, Z., et al. (2018). Pathobiological pseudohypoxia as a putative mechanism underlying myelodysplastic syndromes. Cancer Discov. *8*, 1438–1457.

Hu, Y., and Smyth, G.K. (2009). ELDA: extreme limiting dilution analysis for comparing depleted and enriched populations in stem cell and other assays. J. Immunol. Methods *347*, 70–78.

Ilicic, T., Kim, J.K., Kolodziejczyk, A.A., Bagger, F.O., McCarthy, D.J., Marioni, J.C., and Teichmann, S.A. (2016). Classification of low quality cells from single-cell RNA-seq data. Genome Biol. *17*, 29.

Issaad, C., Croisille, L., Katz, A., Vainchenker, W., and Coulombel, L. (1993). A murine stromal cell line allows the proliferation of very primitive human CD34++/CD38- progenitor cells in long-term cultures and semisolid assays. Blood *81*, 2916–2924.

Ivanova, N.B., Dimos, J.T., Schaniel, C., Hackney, J.A., Moore, K.A., and Lemischka, I.R. (2002). A stem cell molecular signature. Science *298*, 601–604.

Jaatinen, T., Hemmoranta, H., Hautaniemi, S., Niemi, J., Nicorici, D., Laine, J., Yli-Harja, O., and Partanen, J. (2006). Global gene expression profile of human cord blood-derived CD133+ cells. Stem Cells *24*, 631–641.

Jansen, M.W., van der Velden, V.H., and van Dongen, J.J. (2005). Efficient and easy detection of MLL-AF4, MLL-AF9 and MLL-ENL fusion gene transcripts by multiplex real-time quantitative RT-PCR in TaqMan and LightCycler. Leukemia *19*, 2016–2018.

Jones, C.L., Stevens, B.M., D'Alessandro, A., Reisz, J.A., Culp-Hill, R., Nemkov, T., Pei, S., Khan, N., Adane, B., Ye, H., et al. (2018). Inhibition of amino acid metabolism selectively targets human leukemia stem cells. Cancer Cell *34*, 724–740.e4.

Kim, D., Pertea, G., Trapnell, C., Pimentel, H., Kelley, R., and Salzberg, S.L. (2013). TopHat2: accurate alignment of transcriptomes in the presence of insertions, deletions and gene fusions. Genome Biol. *14*, R36.

Klein, A.M., Mazutis, L., Akartuna, I., Tallapragada, N., Veres, A., Li, V., Peshkin, L., Weitz, D.A., and Kirschner, M.W. (2015). Droplet barcoding for single-cell transcriptomics applied to embryonic stem cells. Cell *161*, 1187–1201.

Kluk, M.J., Lindsley, R.C., Aster, J.C., Lindeman, N.I., Szeto, D., Hall, D., and Kuo, F.C. (2016). Validation and implementation of a custom next-generation sequencing clinical assay for hematologic malignancies. J. Mol. Diagn. *18*, 507–515.

Kong, Y., Yoshida, S., Saito, Y., Doi, T., Nagatoshi, Y., Fukata, M., Saito, N., Yang, S.M., Iwamoto, C., Okamura, J., et al. (2008). CD34+CD38+CD19+ as well as CD34+CD38-CD19+ cells are leukemia-initiating cells with self-renewal capacity in human B-precursor ALL. Leukemia *22*, 1207–1213.

Korsunsky, I., Millard, N., Fan, J., Slowikowski, K., Zhang, F., Wei, K., Baglaenko, Y., Brenner, M., Loh, P.R., and Raychaudhuri, S. (2019). Fast, sensitive and accurate integration of single-cell data with Harmony. Nat. Methods *16*, 1289–1296.

Kreso, A., and Dick, J.E. (2014). Evolution of the cancer stem cell model. Cell Stem Cell *14*, 275–291.

Kuntz, E.M., Baquero, P., Michie, A.M., Dunn, K., Tardito, S., Holyoake, T.L., Helgason, G.V., and Gottlieb, E. (2017). Targeting mitochondrial oxidative phosphorylation eradicates therapy-resistant chronic myeloid leukemia stem cells. Nat. Med. *23*, 1234–1240.

Lagadinou, E.D., Sach, A., Callahan, K., Rossi, R.M., Neering, S.J., Minhajuddin, M., Ashton, J.M., Pei, S., Grose, V., O'Dwyer, K.M., et al. (2013). BCL-2 inhibition targets oxidative phosphorylation and selectively eradicates quiescent human leukemia stem cells. Cell Stem Cell *12*, 329–341.

Landt, S.G., Marinov, G.K., Kundaje, A., Kheradpour, P., Pauli, F., Batzoglou, S., Bernstein, B.E., Bickel, P., Brown, J.B., Cayting, P., et al. (2012). ChIP-seq guidelines and practices of the ENCODE and modENCODE consortia. Genome Res. *22*, 1813–1831.

Lange, B., Valtieri, M., Santoli, D., Caracciolo, D., Mavilio, F., Gemperlein, I., Griffin, C., Emanuel, B., Finan, J., Nowell, P., et al. (1987). Growth factor requirements of childhood acute leukemia: establishment of GM-CSF-dependent cell lines. Blood *70*, 192–199.

Langmead, B., and Salzberg, S.L. (2012). Fast gapped-read alignment with Bowtie 2. Nat. Methods *9*, 357–359.

Lapidot, T., Sirard, C., Vormoor, J., Murdoch, B., Hoang, T., Caceres-Cortes, J., Minden, M., Paterson, B., Caligiuri, M.A., and Dick, J.E. (1994). A cell initiating human acute myeloid leukaemia after transplantation into SCID mice. Nature *367*, 645–648.

Lee, K.M., Giltnane, J.M., Balko, J.M., Schwarz, L.J., Guerrero-Zotano, A.L., Hutchinson, K.E., Nixon, M.J., Estrada, M.V., Sanchez, V., Sanders, M.E., et al. (2017). MYC and MCL1 cooperatively promote chemotherapy-resistant breast cancer stem cells via regulation of mitochondrial oxidative phosphorylation. Cell Metab. *26*, 633–647.e637.

le Viseur, C., Hotfilder, M., Bomken, S., Wilson, K., Rottgers, S., Schrauder, A., Rosemann, A., Irving, J., Stam, R.W., Shultz, L.D., et al. (2008). In childhood acute lymphoblastic leukemia, blasts at different stages of immunophenotypic maturation have stem cell properties. Cancer Cell *14*, 47–58.

Li, W.V., and Li, J.J. (2018). An accurate and robust imputation method scImpute for single-cell RNA-seq data. Nat. Commun. *9*, 997.

Liao, Y., Smyth, G.K., and Shi, W. (2014). featureCounts: an efficient general purpose program for assigning sequence reads to genomic features. Bioinformatics *30*, 923–930.

Love, M.I., Huber, W., and Anders, S. (2014). Moderated estimation of fold change and dispersion for RNA-seq data with DESeq2. Genome Biol. *15*, 550.

Lummertz da Rocha, E., Rowe, R.G., Lundin, V., Malleshaiah, M., Jha, D.K., Rambo, C.R., Li, H., North, T.E., Collins, J.J., and Daley, G.Q. (2018). Reconstruction of complex single-cell trajectories using CellRouter. Nat. Commun. *9*, 892.

Macosko, E.Z., Basu, A., Satija, R., Nemesh, J., Shekhar, K., Goldman, M., Tirosh, I., Bialas, A.R., Kamitaki, N., Martersteck, E.M., et al. (2015). Highly parallel genome-wide expression profiling of individual cells using nanoliter droplets. Cell *161*, 1202–1214.

McKenzie, M.D., Ghisi, M., Oxley, E.P., Ngo, S., Cimmino, L., Esnault, C., Liu, R., Salmon, J.M., Bell, C.C., Ahmed, N., et al. (2019). Interconversion between

tumorigenic and differentiated states in acute myeloid leukemia. Cell Stem Cell *25*, 258–272.e9.

Monaco, G., Konopleva, M., Munsell, M., Leysath, C., Wang, R.Y., Jackson, C.E., Korbling, M., Estey, E., Belmont, J., and Andreeff, M. (2004). Engraftment of acute myeloid leukemia in NOD/SCID mice is independent of CXCR4 and predicts poor patient survival. Stem Cells *22*, 188–201.

Nakamura-Ishizu, A., Ito, K., and Suda, T. (2020). Hematopoietic stem cell metabolism during development and aging. Dev. Cell *54*, 239–255.

Ng, S.W., Mitchell, A., Kennedy, J.A., Chen, W.C., McLeod, J., Ibrahimova, N., Arruda, A., Popescu, A., Gupta, V., Schimmer, A.D., et al. (2016). A 17-gene stemness score for rapid determination of risk in acute leukaemia. Nature *540*, 433–437.

Paczulla, A.M., Dirnhofer, S., Konantz, M., Medinger, M., Salih, H.R., Rothfelder, K., Tsakiris, D.A., Passweg, J.R., Lundberg, P., and Lengerke, C. (2017). Long-term observation reveals high-frequency engraftment of human acute myeloid leukemia in immunodeficient mice. Haematologica *102*, 854–864.

Pal, D., Blair, H.J., Elder, A., Dormon, K., Rennie, K.J., Coleman, D.J., Weiland, J., Rankin, K.S., Filby, A., Heidenreich, O., et al. (2016). Long-term in vitro maintenance of clonal abundance and leukaemia-initiating potential in acute lymphoblastic leukaemia. Leukemia *30*, 1691–1700.

Pei, S., Minhajuddin, M., Adane, B., Khan, N., Stevens, B.M., Mack, S.C., Lai, S., Rich, J.N., Inguva, A., Shannon, K.M., et al. (2018). AMPK/FIS1-Mediated mitophagy is required for self-renewal of human AML stem cells. Cell Stem Cell *23*, 86–100.e6.

Pellin, D., Loperfido, M., Baricordi, C., Wolock, S.L., Montepeloso, A., Weinberg, O.K., Biffi, A., Klein, A.M., and Biasco, L. (2019). A comprehensive single cell transcriptional landscape of human hematopoietic progenitors. Nat. Commun. *10*, 2395.

Pieters, R., De Lorenzo, P., Ancliffe, P., Aversa, L.A., Brethon, B., Biondi, A., Campbell, M., Escherich, G., Ferster, A., Gardner, R.A., et al. (2019). Outcome of infants younger than 1 Year with acute lymphoblastic leukemia treated with the interfant-06 protocol: results from an international phase III randomized study. J. Clin. Oncol. *37*, 2246–2256.

Pieters, R., Schrappe, M., De Lorenzo, P., Hann, I., De Rossi, G., Felice, M., Hovi, L., LeBlanc, T., Szczepanski, T., Ferster, A., et al. (2007). A treatment protocol for infants younger than 1 year with acute lymphoblastic leukaemia (Interfant-99): an observational study and a multicentre randomised trial. Lancet *370*, 240–250.

Pollyea, D.A., and Jordan, C.T. (2017). Therapeutic targeting of acute myeloid leukemia stem cells. Blood *129*, 1627–1635.

Potter, M., Newport, E., and Morten, K.J. (2016). The Warburg effect: 80 years on. Biochem. Soc. Trans. *44*, 1499–1505.

Prieto, C., Lopez-Millan, B., Roca-Ho, H., Stam, R.W., Romero-Moya, D., Rodriguez-Baena, F.J., Sanjuan-Pla, A., Ayllon, V., Ramirez, M., Bardini, M., et al. (2018). NG2 antigen is involved in leukemia invasiveness and central nervous system infiltration in MLL-rearranged infant B-ALL. Leukemia *32*, 633–644.

Qiu, J., Gjini, J., Arif, T., Moore, K., Lin, M., and Ghaffari, S. (2021). Using mitochondrial activity to select for potent human hematopoietic stem cells. Blood Adv. *5*, 1605–1616.

Rossi, J.G., Bernasconi, A.R., Alonso, C.N., Rubio, P.L., Gallego, M.S., Carrara, C.A., Guitter, M.R., Eberle, S.E., Cocce, M., Zubizarreta, P.A., et al. (2012). Lineage switch in childhood acute leukemia: an unusual event with poor outcome. Am. J. Hematol. *87*, 890–897.

Rowe, R.G., Lummertz da Rocha, E., Sousa, P., Missios, P., Morse, M., Marion, W., Yermalovich, A., Barragan, J., Mathieu, R., Jha, D.K., et al. (2019). The developmental stage of the hematopoietic niche regulates lineage in MLL-rearranged leukemia. J. Exp. Med. *216*, 527–538.

Saito, Y., Uchida, N., Tanaka, S., Suzuki, N., Tomizawa-Murasawa, M., Sone, A., Najima, Y., Takagi, S., Aoki, Y., Wake, A., et al. (2010). Induction of cell cycle entry eliminates human leukemia stem cells in a mouse model of AML. Nat. Biotechnol. *28*, 275–280.

Sarry, J.E., Murphy, K., Perry, R., Sanchez, P.V., Secreto, A., Keefer, C., Swider, C.R., Strzelecki, A.C., Cavelier, C., Recher, C., et al. (2011). Human acute myelogenous leukemia stem cells are rare and heterogeneous when assayed in NOD/SCID/IL2Rgammac-deficient mice. J. Clin. Invest. *121*, 384–395.

Saygin, C., Matei, D., Majeti, R., Reizes, O., and Lathia, J.D. (2019). Targeting cancer stemness in the clinic: from hype to hope. Cell Stem Cell *24*, 25–40.

Skrtic, M., Sriskanthadevan, S., Jhas, B., Gebbia, M., Wang, X., Wang, Z., Hurren, R., Jitkova, Y., Gronda, M., Maclean, N., et al. (2011). Inhibition of mitochondrial translation as a therapeutic strategy for human acute myeloid leukemia. Cancer Cell *20*, 674–688.

Spencer, J.A., Ferraro, F., Roussakis, E., Klein, A., Wu, J., Runnels, J.M., Zaher, W., Mortensen, L.J., Alt, C., Turcotte, R., et al. (2014). Direct measurement of local oxygen concentration in the bone marrow of live animals. Nature *508*, 269–273.

Struntz, N.B., Chen, A., Deutzmann, A., Wilson, R.M., Stefan, E., Evans, H.L., Ramirez, M.A., Liang, T., Caballero, F., Wildschut, M.H.E., et al. (2019). Stabilization of the max homodimer with a small molecule attenuates myc-driven transcription. Cell Chem. Biol. *26*, 711–723.e4.

Stuart, T., Butler, A., Hoffman, P., Hafemeister, C., Papalexi, E., Mauck, W.M., 3rd, Hao, Y., Stoeckius, M., Smibert, P., and Satija, R. (2019). Comprehensive integration of single-cell data. Cell *177*, 1888–1902.e21.

Subramanian, A., Tamayo, P., Mootha, V.K., Mukherjee, S., Ebert, B.L., Gillette, M.A., Paulovich, A., Pomeroy, S.L., Golub, T.R., Lander, E.S., et al. (2005). Gene set enrichment analysis: a knowledge-based approach for interpreting genome-wide expression profiles. Proc. Natl. Acad. Sci. U S A *102*, 15545–15550.

Takubo, K., Goda, N., Yamada, W., Iriuchishima, H., Ikeda, E., Kubota, Y., Shima, H., Johnson, R.S., Hirao, A., Suematsu, M., et al. (2010). Regulation of the HIF-1alpha level is essential for hematopoietic stem cells. Cell Stem Cell *7*, 391–402.

Tan, Y., and Cahan, P. (2019). SingleCellNet: a computational tool to classify single cell RNA-seq data across platforms and across species. Cell Syst. *9*, 207–213.e2.

Tejedor, J.R., Bueno, C., Vinyoles, M., Petazzi, P., Agraz-Doblas, A., Cobo, I., Torres-Ruiz, R., Bayon, G.F., Perez, R.F., Lopez-Tamargo, S., et al. (2021). Integrative methylome-transcriptome analysis unravels cancer cell vulnerabilities in infant MLL-rearranged B cell acute lymphoblastic leukemia. J. Clin. Invest. *131*, e138833.

Terpstra, W., Ploemacher, R.E., Prins, A., van Lom, K., Pouwels, K., Wognum, A.W., Wagemaker, G., Lowenberg, B., and Wielenga, J.J. (1996). Fluorouracil selectively spares acute myeloid leukemia cells with long-term growth abilities in immunodeficient mice and in culture. Blood *88*, 1944–1950.

van Galen, P., Hovestadt, V., Wadsworth Ii, M.H., Hughes, T.K., Griffin, G.K., Battaglia, S., Verga, J.A., Stephansky, J., Pastika, T.J., Lombardi Story, J., et al. (2019). Single-cell RNA-seq reveals AML hierarchies relevant to disease progression and immunity. Cell *176*, 1265–1281.e24.

Wang, Y., Liu, Y., Malek, S.N., Zheng, P., and Liu, Y. (2011). Targeting HIF1alpha eliminates cancer stem cells in hematological malignancies. Cell Stem Cell *8*, 399–411.

Witkowski, M.T., Dolgalev, I., Evensen, N.A., Ma, C., Chambers, T., Roberts, K.G., Sreeram, S., Dai, Y., Tikhonova, A.N., Lasry, A., et al. (2020). Extensive remodeling of the immune microenvironment in B cell acute lymphoblastic leukemia. Cancer Cell *37*, 867–882.e12.

Zilionis, R., Nainys, J., Veres, A., Savova, V., Zemmour, D., Klein, A.M., and Mazutis, L. (2017). Single-cell barcoding and sequencing using droplet microfluidics. Nat. Protoc. *12*, 44–73.

STAR★METHODS

KEY RESOURCES TABLE

REAGENT or RESOURCE	SOURCE	IDENTIFIER
Antibodies		
Anti-human CD19 PE (4G7)	Biolegend	Cat#392505; RRID: AB_2750096
Anti-human CD45 FITC (HI30)	BD Biosciences	Cat#561865; RRID: AB_10896120
Anti-human CD33 APC (P67.6)	BD Biosciences	Cat#340474; RRID: AB_400518
Anti-human CD34 PE-Cy7 (8G12)	BD Biosciences	Cat#348791; RRID: AB_400381
Anti-human CD38 PE	BD Biosciences	Cat#347687; RRID: AB_400341
Anti-human CD45 APC	BD Biosciences	Cat#555485; RRID: AB_398600
Anti-human CD45RA FITC	BD Biosciences	Cat#347723; RRID: AB_400343
Anti-human CD90 BV605	BD Biosciences	Cat#562685; RRID: AB_2744468
Anti-mouse CD45.1-APC-Cy7 (A20)	BioLegend	Cat#110716; RRID: AB_313505
Anti-Ki67 APC	Biolegend	Cat#350513; RRID: AB_10959326
Anti-c-MYC	Cell Signal	Cat#9402; RRID: AB_2151827
Anti-beta-actin (8H10D10)	Cell Signal	Cat#3700; RRID: AB_2242334
Bacterial and virus strains		
Stbl3 E. coli	Thermo Fisher	C737303
Biological samples		
Patient derived xenografts	This paper	N/A
Primary patient leukemia cells	This paper	N/A
Chemicals, peptides, and recombinant proteins		
May-Grunwald stain	Sigma-Aldrich	MG500
Giemsa stain	Sigma-Aldrich	R03055
Doxycycline hyclate	Sigma-Aldrich	D9891
Recombinant human stem cell factor	R and D Systems	255-SC-010
Recombinant human FLT3-ligand	R and D Systems	308-FK-005
Recombinant human thrombopoietin	R and D Systems	288-TP-005
Recombinant human interleukin-7	R and D Systems	207-IL-005
Mitotracker green	Thermo Fisher	CAS: 201860-17-5
IBET-151	SelleckChem	CAS: 1300031-49-5
3-bromopyruvate	Sigma	CAS: 113-59-3
Dichloroacetate	Sigma	CAS: 2156-56-1
Echinomycin	Tocris	CAS: 512-64-1
Tigecycline	LKT Labs	CAS: 220620-09-7
CellRox Deep Red	Thermo Fisher	C10422
Critical commercial assays		
Seahorse Mito Stress Test	Agilent	103015-100
CellTiter Glo	Promega	G7570
Deposited data		
Raw data	This paper	Sequence Read Archive SRA: phs002492
Analyzed data	This paper	Gene Expression Omnibus GEO: GSE147862
Experimental models: Cell lines		
MV4; 11	ATCC	ATCC CRL-9591; RRID:CVCL_0064
RS4; 11	ATCC	ATCC CRL-1873: RRID:CVCL_0093
HEK293	ATCC	ATCC CRL-3216; RRID:CVCL_0045
MS5 mouse bone marrow stroma	N/A	RRID:CVCL_2128

(*Continued on next page*)

Continued

REAGENT or RESOURCE	SOURCE	IDENTIFIER
Experimental models: Organisms/strains		
NSG mice	Jackson Laboratory	Strain #:005557; RRID:BCBC_4142
Oligonucleotides		
Human *MLL-AF4* forward: MLL-F1 5′-CG CCTCAGCCACCTACTACAG-3′	Jansen et al. (2005)	N/A
Human *MLL-AF4* reverse: AF4-R1 5′-AGG TCGTCTTCGAGCATGGA-3′	Jansen et al. (2005)	N/A
Human *GAPDH* forward: GAPDH-F 5′-GTC TCCTCTGACTTCAACAGCG-3′	This paper	N/A
Human *GAPDH* reverse: GAPDH-R 5′-ACC ACCCTGTTGCTGTAGCCAA-3′	This paper	N/A
Recombinant DNA		
pPAX2	Addgene	12260
pCMV-VSV-G	Addgene	8454
pDONR223_MYC_WT	Addgene	82927
pCW57.1	Addgene	41393
Software and algorithms		
SingleCellNet	Tan and Cahan (2019)	https://github.com/pcahan1/singleCellNet/
Bowtie2	Langmead and Salzberg (2012)	http://bowtie-bio.sourceforge.net/bowtie2/index.shtml
TopHat2	Kim et al. (2013)	https://ccb.jhu.edu/software/tophat/index.shtml
Indrops pipeline	Klein et al. (2015)	https://github.com/indrops/indrops
Drop-seq pipeline	Macosko et al. (2015)	http://mccarrolllab.com/dropseq
GSEA	Subramanian et al. (2005)	https://www.gsea-msigdb.org/gsea/index.jsp
AQUAS	N/A	https://github.com/kundajelab/chipseq_pipeline
CellRouter	Lummertz da Rocha et al., 2018	https://github.com/edroaldo/cellrouter
Seurat	Stuart et al. (2019)	https://github.com/satjialab/seurat
Bcl2fastq	Illumina	https://support.illumina.com/sequencing/sequencing_software/bcl2fastq-conversion-software.html
Umis	N/A	https://github.com/vals/umis

RESOURCE AVAILABILITY

Lead contact

Further information and requests for resources and reagents should be directed to and will be fulfilled by the lead contact, Grant Rowe (grant_rowe@dfci.harvard.edu).

Materials availability

Plasmids generated in this study will be deposited to Addgene prior to the date of publication or are available upon request from the lead contact.

Data and code availability

- scRNA-seq, CITE-seq, ChIP-seq, and bulk RNA-seq (processed human data) have been deposited in Gene Expression Omnibus and are publicly available as of the date of publication. All raw sequencing data derived from human samples have been deposited in the Sequence Read Archive and are available through request to the NIH Database of Genotypes and Phenotypes as of the date of publication. Accession numbers are listed in the key resources table.

- This paper does not report original code.
- Any additional information required to reanalyze the data reported in this paper is available from the lead contact upon request.

EXPERIMENTAL MODEL AND SUBJECT DETAILS

Animal models

All studies were approved by the Boston Children's Hospital Institutional Animal Care and Use Committee. Eight-week-old unconditioned female NSG mice (Jackson Laboratory stock 005557) were transplanted with the indicated cell sources at the indicated doses by tail vein injection. Mice were randomly allotted to each experimental group. Mice were followed to the onset of terminal leukemia as assessed by the onset of morbidity, judged by investigators blinded to the experimental conditions. Mice were housed in autoclaved cages with sterilized food and water.

For tigecycline treatment, mice were treated for two days with 25 mg/kg tigecycline (LKT labs) dissolved in 10% DMSO/90% (5% Kleptose HPB in PBS). The dose was then escalated to 50 mg/kg for three days and then 100 mg/kg for 7 days. After 48 hours, mice were euthanized for endpoint analysis. For IBET-151 treatment, mice were treated with IBET-151 (R and D Systems) at a dose of 30 mg/kg in 10% DMSO/90% (5% Kleptose HPB in PBS) for 5 days per week for two weeks followed by euthanization for analysis. For *in vivo* dicholoroacetate treatment, mice were engrafted with the indicated leukemias and dichloroacetate added to the drinking water to target a dose of 100 mg/kg/day based on average daily water consumption (Bonnet et al., 2007). Echinomycin was given at 10 μg/kg per day for five days on, two days off, five days on (10 total treatments per mouse) (Wang et al., 2011).

Human subjects

Use of primary human cells, PDX cells, and cell lines was reviewed and approved by the Boston Children's Hospital Institutional Review Board. All primary patient and PDX specimens were procured following informed consent. Specimens of both sexes were included. Sex and age of specimens included in this study is provided in Table S1. Human cell lines were obtained from the ATCC.

Cell culture

Patient derived leukemia cells were cultured on MS5 stromal cells in the presence of 50 ng/mL recombinant human stem cell factor (SCF), 50 ng/mL recombinant human thrombopoietin (TPO), 10 ng/mL recombinant human FLT3 ligand (FLT3L), and 10 ng/mL recombinant human interleukin-7 (IL-7, all from R and D Systems) in Myelocult H5100 (Stem Cell Technologies) supplemented with 1% penicillin/streptomycin (Issaad et al., 1993) with modifications based on (Doulatov et al., 2010) to facilitate lymphoid cell growth; i.e., without horse serum or hydrocortisone (Issaad et al., 1993). Leukemia 1/*MLL-AF4* was most amenable to *in vitro* culture and so was used for most culture-based experiments. For *in vitro* LDA experiments, 5,000 MS5 cells were plated in wells of gelatin-coated Nunc 96 well plates (Fisher Scientific) with cytokines 48 hours prior to FACS-based sorting of leukemia cells directly into the wells.

Human MV4; 11 and RS4; 11 cells (ATCC) were cultured in RPMI with 10% fetal calf serum supplemented with penicillin and streptomycin.

As indicated in Table S1, some specimens were subjected to focused somatic mutation analysis (Rapid Heme Panel (Kluk et al., 2016)).

METHOD DETAILS

Flow cytometry and cell sorting

Data were acquired on either BD LSR Fortessa or LSR II Instruments (BS Biosciences). Cells were sorted on a BD FACS Aria (BD Biosciences) with a 100 μm nozzle. Mitotracker Green and CellRox were purchased from Thermo. Mitotracker Green was used at 300 n*M* and all experiments included verapamil at 50 μ*M* with incubation at 37°C for 30 minutes prior to analysis (de Almeida et al., 2017). Antibodies used are listed in the key resources table.

Morphology

For morphologic analysis, leukemia cells were spun onto slides and stained with May-Grunwald and Giemsa stains (Sigma) sequentially. Transmission electron microscopy was performed at the electron microscopy core at Harvard Medical School.

Recombinant DNA

The human *MYC* cDNA was purchased from Addgene (pDONR223_MYC_WT, a gift from Jesse Boehm and Matthew Meyerson and David Root (plasmid # 82927; http://n2t.net/addgene:82927; RRID: Addgene_82927). The *MYC* cDNA was cloned into the pCW57.1 vector (gift from David Root (Addgene plasmid # 41393; http://n2t.net/addgene:41393; RRID:Addgene_41393) using LR clonase (Thermo). The purified plasmid was used to generate lentivirus in HEK-293T cells, which was used to transduce MV4; 11 cells. A stable transduced polyclonal line was selected with 0.5 μg/mL puromycin (Thermo). The *MYC* cDNA was also cloned into pINDUCER21 (ORF-EG) which was a gift from Stephen Elledge and Thomas Westbrook (Addgene plasmid # 46948; http://n2t.net/addgene:46948; RRID: Addgene_46948) to generate lentivirus for transduction of B-ALL patient derived xenografts. Gene expression was confirmed by Western blotting following doxycycline exposure.

Western blotting

Antibodies are listed in the key resources table. After lysis in SDS sample buffer, proteins were resolved on 4–20% gradient polyacrylamide gels (BioRad) using the Tris buffer system. Proteins were transferred to PVDF membranes, and membranes were blocked and probed per the manufacturer's protocol. Signal was developed using the ECL system (Pierce) and detected by exposure to radiography film. Western blot band intensities were quantified with ImageJ.

Seahorse Mito Stress assay

The Seahorse assays were performed using the Agilent Seahorse XF Cell Mito Stress Test kit using injections of 1 μ*M* oligomycin, 1 μ*M* carbonyl cyanide-4 (trifluoromethoxy) phenylhydrazone (FCCP) and 0.5 μ*M* each of antimycin A and rotenone at the intervals indicated. Prior to analysis, cells were equilibrated for one hour in Mito Stress medium supplemented with 1 m*M* pyruvate, 10 m*M* glucose, and 2 m*M* L-glutamine. The instrument is located at the Seahorse Core at Brigham and Women's Hospital. All assays were normalized based on the number of viable cells included following drug pre-treatment to control for effects of drug treatment on viability. For assays using primary leukemia cells, cells were cultured on MS5 stroma for 72 hours prior to B-ALL cell purification by human CD45 bead enrichment (Miltenyi) followed by Seahorse Mito Stress analysis.

Long-term culture initiating cell assay

The indicated populations were sorted by FACS and placed onto MS5 stroma with cytokines either under normoxia (21%) or hypoxia (5%) for four weeks. At that time, viable, human $CD45^+$ cells were sorted into 96-well plates at the indicated doses. After two weeks, outgrowths were blindly scored.

Reverse transcription PCR

RNA was isolated from the indicated cell populations using Trizol reagent. cDNA was prepared using the miScript II kit (Qiagen). Primers are listed in the key resources table. *MLL-AF4* primers were reported previously (Jansen et al., 2005). Band were visualized following gel electrophoresis and ethidium bromide staining. Product specificity was confirmed by Sanger sequencing.

Single cell RNA sequencing

For scRNA-seq using the Seq-Well platform, 20,000 cells were applied to one Seq-Well array pre-loaded with mRNA capture beads (ChemGenes) as previously described (Gierahn et al., 2017). The arrays were sealed with a polycarbonate membrane with a 0.01 μm pore size permissive of exchange of buffers but not macromolecules. Following cell lysis, transcript hybridization, and bead recovery by buffer exchange, reverse transcription was performed using Maxima H Minus Reverse Transcriptase (ThermoFisher) with random second-strand synthesis was performed to generate double stranded cDNA. Exonuclease I treatment (New England Biolabs) was performed to remove excess primers. PCR was performed using the following primer sequence 5′ – AAGCAGTGGTATCAACGCAGAGT – 3′ and the KAPA HiFi PCR Mastermix (Kapa Biosystems) with 2,000 beads per 50 μL reaction volume. Sequencing libraries were generated using the Illumina Nextera XT protocol using custom N700 sequencing indices. Libraries were sequenced using Next-Seq 75 cycle high output sequencing kits with 20 base read 1 sequence and 50 base read 2 sequence.

For inDrop-seq, FACS-sorted cells at 100,000 cells/mL were encapsulated in 2–3 nL droplets using a microfluidic device (located at the Harvard Medical School Single Cell Core) and the libraries were made following a previously described protocol (Klein et al., 2015; Zilionis et al., 2017), with the following modifications in the primer sequences. RT primers on hydrogel beads- 5′CGATTGATCAACGTAATACGACTCACTATAGGGTGTCGGGTGCAG[bc1,8nt]GTCTCGTGGGCTCGGAGATGTGTATAAGAGACAG [bc2,8nt]NNNNNNTTTTTTTTTTTTTTTTTTTV- 3′.

R1-N6 primer sequence (step 151 in the library prep protocol in (Zilionis et al., 2017))- 5′TCGTCGGCAGCGTCAGATGTG TATAAGAGACAGNNNNNN-3′.

PCR primer sequences (steps 157 and 160 in the library prep protocol in (Zilionis et al., 2017))- 5′-AATGATACGGCGACCACCGA GATCTACACXXXXXXXXTCGTCGGCAGCGTC-3′, where XXXXXX is an index sequence for multiplexing libraries.

5′-CAAGCAGAAGACGGCATACGAGATGGGTGTCGGGTGCAG-3′.

With these modifications in the primer sequences, custom sequencing primers are no longer required. Reverse transcription was performed at 50°C for two hours followed by 15 minutes at 70°C. scRNA-seq was library preparation was performed by the Single Cell Core at Harvard Medical School, Boston, MA using the NEBNext mRNA Second Strand Synthesis Module with random hexamer priming.

For CITE-seq, cells were pre-stained with barcoded antibodies against CD38 and CD34 (Biolegend) and inDrop libraries were prepared as above.

Bulk RNA sequencing library preparation

Cells were sorted by FACS and lysed in Trizol reagent (Thermo). RNA was isolated using RNAeasy columns (Qiagen) and low input libraries prepared in collaboration with the Molecular Biology Core at the Dana-Farber Cancer Institute using the NEBNext Single Cell/ Low Input RNA Library Prep Kit for Illumina (New England Biolabs).

Data analysis

InDrop single-cell RNA-sequencing

Raw sequencing reads were processed using the inDrop pipeline (https://github.com/indrops/indrops) using default parameters (Klein et al., 2015) The hg38 reference genome was used for alignment of sequencing reads. We used scImpute to account for dropout rates in single-cell RNA-seq data and obtain an imputed count matrix that was used for all downstream analysis described (Li and Li, 2018). We used scImpute with the parameter 'Kcluster = 10'. To analyze imputed single cell inDrop data we performed quality control, dimensionality reduction, clustering and differential expression analysis using CellRouter (Lummertz da Rocha et al., 2018). For this leukemia, we applied the following quality control metrics: all genes that were not detected in at least 20 cells were excluded. All cells with less than 200 genes detected were also excluded. As expression of ribosomal or mitochondrial genes is indicative of technical variation in single-cell RNA-seq data we also removed cells where the proportion of the transcript counts derived from mitochondrial genes was greater than 10% (Ilicic et al., 2016). After such quality control of the imputed count matrix, we retained 5,153 cells with a median of 15,214 genes detected per cell.

Integrated analysis of leukemia samples

We used Seurat 4.0 to integrate our leukemia samples, which were generated using the inDrop and SeqWell technologies (Stuart et al., 2019). Briefly, we individually normalized each sample using the LogNormalize() function, and identified the 3000 most variable genes in each dataset based on a variance stabilizing transformation. Then, we used the FindIntegrationAnchors() function followed by the IntegrateData() function from Seurat to integrate the datasets. Following data integration, we performed a cell cycle regression of S and G_2/M phase scores, which preserves the cell cycle signal associated with cell differentiation. We then performed UMAP and clustering analysis using the first 20 principal components. For clustering, we used 20 principal components in the function FindNeighbors(), and defined the parameter 'resolution' of the FIndClusters function as 0.25. Differential expression analysis was used to identify cluster-specific genes by selecting those more highly expressed in each cluster based on a fold change cutoff of 0.2.

Seq-Well single-cell RNA-sequencing

Read alignment was performed as described (Macosko et al., 2015). Briefly, for each NextSeq sequencing run, raw sequencing data was converted to FASTQ files using bcl2fastq2 that were demultiplexed by Nextera N700 indices corresponding to individual samples. Reads were first aligned to hg19, and individual reads were tagged according to the 12-bp barcode sequence and the 8-bp UMI contained in read 1 of each fragment. Following alignment, reads were binned and collapsed onto 12-bp cell barcodes that corresponded to individual beads using Drop-seq tools (http://mccarrolllab.com/dropseq). Barcodes were collapsed with a single-base error tolerance (Hamming distance = 1), with additional provisions for single insertions or deletions. An identical collapsing scheme (Hamming distance = 1) was then applied to UMIs to obtain quantitative counts of individual mRNA molecules. We also used scImpute to impute the raw counts matrix obtained, with the parameter of 'Kcluster = 6'. For this leukemia, we removed all genes expressed in less than 10 cells and also removed all cells expressing less than 500 genes. Cells with transcript counts derived from mitochondrial genes larger than 10% were also removed. After QC, we retained 6,320 cells with a median of 2,588.5 genes detected per cell.

Normalization

Both inDrop and Seq-Well data were analyzed with CellRouter. In CellRouter, transcript counts are normalized using a global scaling normalization method that normalizes expression measurements for each cell by the total expression, multiplied by a scale factor of 10,000, and log-transformed the result.

Re-analysis publicly available leukemia samples

We re-analyzed scRNA-seq data from four Ph+ samples at diagnosis generated by Witkowski et al., 2020, GEO accession number GSE134759. Briefly, we subset CD19 + cells by selecting individual cells whose normalized expression level is higher than the mean expression of all cells expressing CD19 above zero. This approach resulted in 1,452 CD19 + single cells from four Ph + samples, which were integrated using Seurat as described above. UMAP and clustering analysis were performed using 20 principal components and the parameter "resolution" of the FindClusters function was set to 0.5.

We also re-analyzed data generated by Candelli et al. (2022), accession number EGAS00001003986. From this dataset, we analyzed 13,250 individual cells after quality control (genes expressed in less than 25 cells and cells expressing less than 300 genes were removed from all downstream analysis). These samples were integrated with Seurat as previously described. UMAP and clustering analysis were performed using 17 principal components and the parameter "resolution" of the FindClusters function was set to 0.75.

Finally, we reanalyzed a dataset generated by Chen et al. (2021), composed of 88,228 single cells from 18 *MLL*-r B-ALL patient samples for which a Seurat object was downloaded from Synapse at https://www.synapse.org/. To integrate these samples we used the algorithm Harmony (Korsunsky et al., 2019). After integration, UMAP and clustering analysis were performed using 20 principal components and the parameter "resolution" of the FindClusters function was set to 0.5. Regression of the difference between cell cycle scores for the S-phase and G_2/M-phase was performed for the three studies mentioned above.

SingleCellNet analysis

We downloaded scRNA-seq data from the GEO accession number GSE116256 (van Galen et al., 2019). This study performed a random sampling of hematopoietic cells in the normal and leukemic bone marrow (BM) ecosystem. We reanalyzed five healthy BM samples published with this study and used cell types identified by the authors to train machine learning models of cell type identity of BM cells using SingleCellNet. After training, we classified each single cell in our leukemia samples as belonging to any of the classes in our training dataset. Additionally, we also used the dataset generated by Pellin et al., (2019) as training dataset to classify leukemia samples.

Signature scores

We downloaded gene lists from https://www.gsea-msigdb.org/gsea/msigdb. Specifically, we downloaded the following gene sets: HALLMARK_MYC_TARGETS_V1.txt, HALLMARK_OXIDATIVE_PHOSPHORYLATION.txt, JAATINEN_HEMATOPOIETIC_STEM_CELL_UP, and IVANOVA_HEMATOPOIESIS_STEM_CELL.txt. Then, we used CellRouter to calculate signature scores for each cell and plotted the distribution of these scores.

For the signature analysis of Candelli et al. (2022), we used data from 15 peripheral blood samples of infants with MLL-rearranged ALL (EGA accession number EGAS00001003986). We considered GSEA gene sets 'HALLMARK_OXIDATIVE_PHOSPHORYLATION', 'HALLMARK_GLYCOLYSIS', and 'HALLMARK_HYPOXIA' and used them to calculate a module score for each gene set as described in Candelli et al., (2022). Annotation of resistant (LIC) and sensitive (differentiated blasts) populations is as in Candelli et al., (2022).

CITE-seq

We converted binary files from the Illumina run to fastq files corresponding to 4 reads of indrops3 library with bcl2fastq/2.18.0.12 without read trimming. https://support.illumina.com/sequencing/sequencing_software/bcl2fastq-conversion-software.html. We created a single fastq file containing cell and sample barcode information in the header of the read with umis fastqtransform https://github.com/vals/umis. We then wrote a custom python script to count antibody barcodes and assign the counts to a proper cell/sample pair. The input parameters of the script were antibody barcodes (tags), a fastq file from step2, and a list of sample barcodes. We ran the script using the wrapper https://github.com/hbc/rowe2020_indrop_citeseq_hbc03948/blob/master/04.cite_seq_count.sh.

Bulk RNA-sequencing

Fastq files containing single-end RNA-seq reads were aligned with Tophat 2.0.12 against the UCSC hg38 reference genome using Bowtie 2.2.4 with default settings (Kim et al., 2013; Langmead and Salzberg, 2012). Gene level counts were obtained using the subRead featureCounts program (v1.5.1) using the parameter "–primary" and gene models from the UCSC hg38 Illumina iGenomes annotation package (Liao et al., 2014). Differential expression analysis was performed with the DESeq2 package using 'ashr' as a shrinkage estimator for the $\log_2$ fold changes (Love et al., 2014). Genes with $\log_2$ fold changes > 0.5 and $P_{adj} < 0.05$ were considered significantly differentially expressed. For visualization of gene expression patterns and hierarchical clustering, read counts were normalized using size factors as available by the DESeq2 package and visualized using the pheatmap package (Love et al., 2014).

ChIP-seq

ChIP-seq was performed as previously described and in accordance with the Encode guidelines (Chapuy et al., 2013; Landt et al., 2012). We used 100×10^6 exponentially growing MV4; 11 or RS4; 11 cells. Cells were fixed with 1% formaldehyde for 10 minutes at room temperature and then quenched with 125 m*M* glycine for 5 minutes and washed with PBS. Nuclei were isolated using the Nucleo EZ isolation buffer (Sigma) and resuspended in 10 m*M* Tris-HCl, pH 8.0, 1 m*M* EDTA, 0.1% SDS with 1x HALT protease inhibitor (ThermoFisher). Chromatin was fragmented by sonication on an E220 Covaris focused sonication machine using the parameters of 140 mV, 5% duty factor, 200 cycles/burst for 14 minutes. The following antibodies were used for ChIP: MYC (Cell Signaling 9402). ChIP-seq libraries were prepared using Swift S2 Acel reagents (Swift 21096) on a Beckman Coulter Biomek i7 liquid handling platform from approximately 1 ng of DNA according to manufacturer's protocol and using 14 cycles of PCR amplification. Sequencing libraries were quantified by Qubit fluorometer and Agilent TapeStation 2200. Library pooling and indexing was evaluated by shallow sequencing on Illumina MiSeq. Subsequently, libraries were sequenced on NovaSeq targeting 40 million 100 bp read pairs by the Molecular Biology Core facilities at the Dana-Farber Cancer Institute. Sequencing reads were processed using the AQUAS pipeline (https://github.com/kundajelab/chipseq_pipeline) with minor modifications and according to the ENCODE3 guidelines. Reads were aligned to the hg38 genome build using BWA-ALN and peaks were called using MACS2.

QUANTIFICATION AND STATISTICAL ANALYSIS

Statistical testing was performed as described in the figure legends using either Prism (Graphpad) or Excel (Microsoft). For each experiment, n and precision measures are provided in the figure legends. Power calculations were used to estimate cohort sizes for *in vivo* experiments. P-values are shown in the figures or are presented in the figure legends.